Title
CYCLOTRON ECHOES IN Cs VAPOR

Author
Shaner, John Wesley.

Publication Date
1969-10-01

Thesis/dissertation

UCRL-19085
cy. 2

CYCLOTRON ECHOES IN Cs VAPOR

John Wesley Shaner
(Ph. D. Thesis)

October 1969

AEC Contract No. W-7405-eng-48

LAWRENCE RADIATION LABORATORY
UNIVERSITY of CALIFORNIA BERKELEY

DISCLAIMER

CONTENTS

ABSTRACT v

I. INTRODUCTION 1

II. TWO-PULSE ECHOES 7

A. Assumptions 7

B. Interaction 7

C. Simple Model 10

D. Exact Description 19

E. Potpourri 31

F. Relation to Spin Echoes 36

III. THREE-PULSE ECHOES 38

IV. EXPERIMENTS AND DISCUSSION 51

ACKNOWLEDGEMENTS 73

APPENDIX A 74

APPENDIX B 77

APPENDIX C 90

APPENDIX D 95

REFERENCES 97

CYCLOTRON ECHOES IN Cs VAPOR

John Wesley Shaner

Inorganic Materials Research Division, Lawrence Radiation Laboratory, and Department of Physics, University of California, Berkeley, California

ABSTRACT

Cyclotron echoes have been studied in a weakly ionized cesium plasma in a magnetic field. The behavior of the multiple echoes following two resonant microwave pulses (two-pulse echoes) and those following three resonant microwave pulses (three-pulse echoes) are shown for various pulse spacings and neutral Cs densities. These results are compared with various theoretical models. On the basis of this comparison, the velocity dependence of the electron-neutral collision frequency is chosen as the mechanism for two-pulse echo generation. Several mechanisms are invoked to explain the three-pulse echoes, including scattering without diffusion and diffusion across flux lines. A detailed comparison is made between the results from these models and the experimental results.

"... now Echo always
says the last thing she hears, and nothing further."

Ovid[1]

I. INTRODUCTION

According to Bulfinch,[2] Echo was well known to Greeks and Romans over two centuries ago. She was the nymph who distracted Hera with her chatter while Zeus, who was amusing himself with the other nymphs, made good his retreat. When Hera found out this scheme, she punished Echo by limiting her speech to those words she had just heard. With this curse, Echo had the further misfortune to meet by chance and fall in love with Narcissus. When this self-centered youth repulsed her advances, Echo ran away to the mountains to hide her shame. In her grief her flesh shrank away until only her voice remained to reply to all who called to her in the mountains.

This was undoubtedly only a formal description of the phenomenon of echoes, which had amused men since our simian ancestors first heard their screeches echoed in mountainous areas. Unfortunately the first observation went unpublished, so it cannot be properly referenced.

No echo phenomena other than returning waves bounced off of reflecting surfaces were observed until 1950, when Hahn[3] reported the first nuclear spin echoes. These echoes were shown to be useful in the study of the various relaxation mechanisms affecting nuclear moments. Soon thereafter echoes were observed in several other quantum systems involving a small number of levels. The list now includes transitions in electron paramagnetic,[4] nuclear quadrupole,[5] electric dipole,[6-7] molecular rotational,[8] molecular vibrational,[9] and atomic hyperfine[10] systems.

In a paper by Feynman et al.[11] the fact that all two level quantum systems can be cast into the same form as the nuclear spin 1/2 system is proved. Also, it is well known that when proper statistical averages are taken in a quantum mechanical spin system, the resulting equation of motion for the macroscopic moment is the same as that obtained from classical theory.[12] Therefore, to the extent that these quantum systems can be cast into a two-level form, they can all be explained by Hahn's original treatment.[3]

More recently similar echo phenomena have been observed in the Landau levels of a free electron gas, and in several systems with collective modes. The former are called cyclotron echoes.[13] The latter include ferrimagnetic modes,[14] and electron[15] and ion[16] plasma waves.

What all of these systems have in common is an inhomogeneously broadened spectrum (frequency or velocity), defined as follows: there is some subensemble of the system, including all its interactions with the whole system, for which the spectral width of the subensemble is less than that of the whole system. Also some condition on how wildly the inhomogeneous broadening mechanism varies with time is necessary. A sufficient, though not necessary condition for all the systems in which echoes have been observed is that the frequency of any oscillator is constant for the duration of the echo experiment. Less strict conditions are shown to be sufficient in Appendix D. Examples of such a broadening mechanism for localized oscillators, like spins, are an inhomogeneous magnetic field, strain broadening, and doppler broadening. In the electron plasma wave echoes, the spectrum can be thought of as the whole electronic velocity distribution. Any subsystem, for example, that part that is affected by the Landau damping, has a smaller spread in phase space, and therefore a smaller spectral width, according to the above definition.

In addition, there may be a homogeneous broadening mechanism acting on the system. By this is meant the spectral width of a single oscillator plus its interactions. This mechanism ultimately determines the decay rate of the echo. Therefore, a study of this decay rate is a study of the homogeneous broadening.

When a signal comes from such an inhomogeneously broadened system it is usually an average over the whole line weighted by a spectral distribution function, $g(\Omega)$ (or $f(\vec{v})$ for the plasma wave echo). If the inhomogeneous line has a width Δ, such an average decays with a characteristic time $T_2^* = 1/\Delta$. Thus, any signal arising from an average over the whole spectrum will decay with this time constant. However, a particular isochromat (a collection of oscillators with the same center frequency for their homogeneously broadened lines) continues its coherent motion in phase space for a time $T_2 = 1/\delta$ where δ is the homogeneous spectral width. Therefore the inhomogeneously broadened line condition ($T_2^* < T_2$) implies that although the macroscopic signal decays with a time constant T_2^*, the microscopic dynamics of each isochromat remains coherent for a time T_2, and therefore the system contains more information between these two times than the macroscopic signal would indicate. All of these echo phenomena use some form of trickery to extract this information, thereby yielding a measure of T_2.

The first observation of cyclotron echoes was made by Hill and Kaplan[13] in 1965. Their system consisted of the free electrons in a weakly ionized plasma in an inhomogeneous magnetic field. The magnetic field was such that the electron cyclotron frequency was resonant with the microwave fields. X-band microwave pulses, ten nanoseconds in duration were directed at the system in the time sequence shown in Fig. 1.

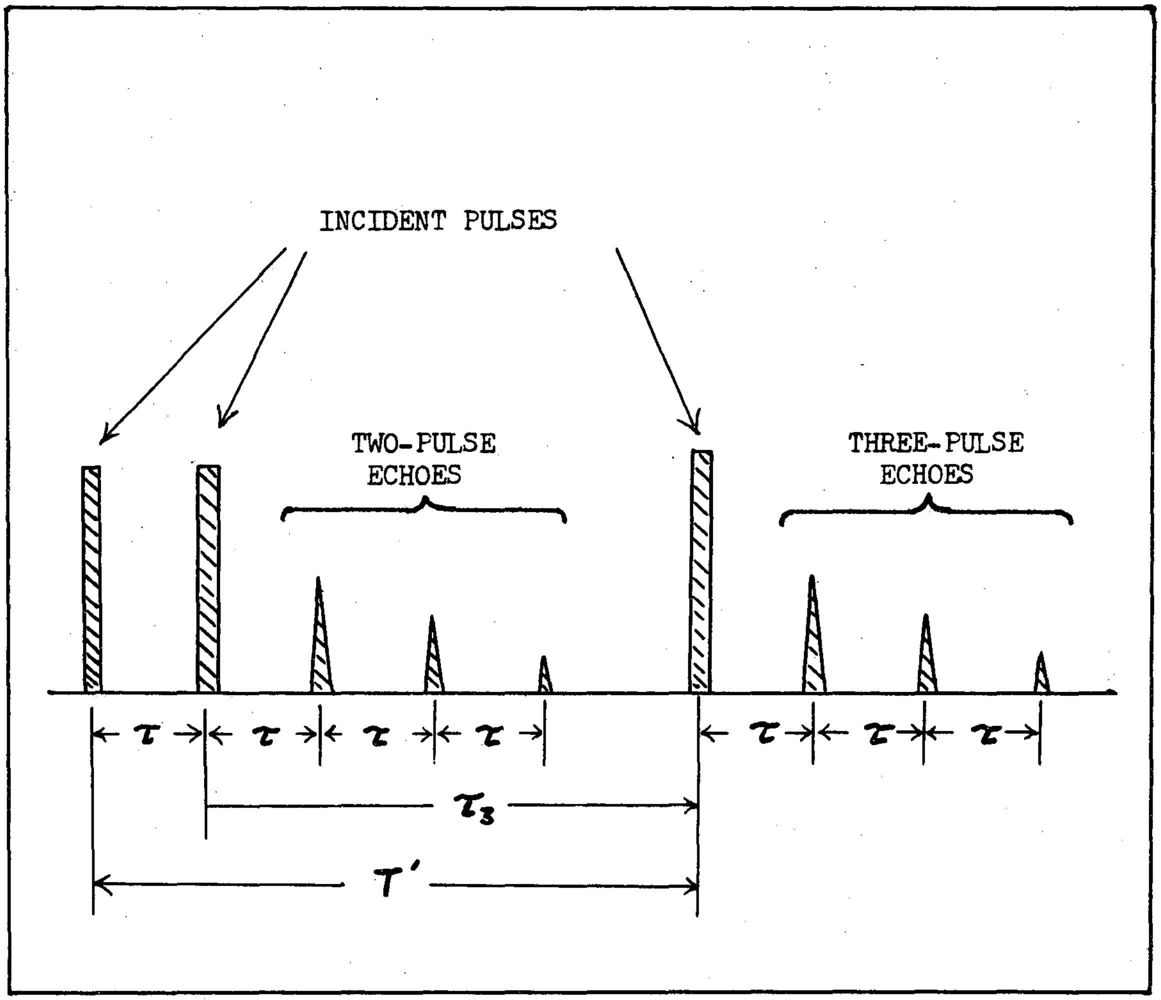

Figure 1. Two- and three-pulse cyclotron echo timing sequence.

Multiple echoes, equally spaced in the time domain were radiated from the system after both the second (two-pulse echoes) and the third (three-pulse echoes) microwave pulses. These echoes were extremely powerful, sometimes as large as 0.1 milliwatt. The plasmas in which cyclotron echoes were observed were Argon, Neon, and Nitrogen, with typical neutral densities of 10^{14}-10^{15} cm^{-3} (3-30×10^{-3} Torr) and electron densities of 10^{8}-10^{9} cm^{-3}. Echoes were also observed somewhat later in a strongly ionized Cs plasma.[21]

These observations resulted in several theoretical papers discussing echo forming mechanisms. Included in these mechanisms were the nonlinear interaction of the electron with the microwave fields,[17] the relativistic electron mass shift,[18] and the velocity dependence of the collision frequency.[19] The first two mechanisms were calculated to give echo powers proportional to $(v/c)^2$ where v is the electronic velocity, and c is the speed of light, but no numbers were reported for an absolute magnitude of the echo power. When such a number is calculated, it turns out orders of magnitude too small to explain the observed echoes. The velocity dependent collision frequency mechanism was shown to give the correct order of magnitude for the echo amplitude, but no detailed comparisons of theory with data have yet been published. In this work, we present such a comparison for a weakly ionized cesium plasma.

The only theoretical mechanism which has even predicted a correct order of magnitude for the three pulse echoes involves the diffusion of electrons across flux lines in the plasma.[20] Again, no detailed comparison of experimental data with this theory have been published.

In this report, the velocity dependent collision and other mechanisms for two-pulse echoes are discussed in Chapter II. Also, in that chapter detailed calculations of the two-pulse echo behavior for the weakly ionized Cs plasma are presented. In Chapter III, three-pulse echo mechanisms are discussed. Finally, in Chapter IV the experiments are discussed and the experimental results are compared with the theories of Chapters II and III.

II. TWO-PULSE ECHOES

A. Assumptions

Several assumptions shall be made at the outset concerning the system considered. First, we assume a linear interaction of the plasma electrons with the resonant microwaves. This assumption will be reasonable so long as the incident microwave pulse power is not too large. When the pulse power gets so large that the resulting electron velocity cannot be neglected when compared to the speed of light, this first assumption breaks down. Of course, this is equivalent to ignoring all relativistic effects. The consequences of large pulse powers are discussed in Section IIE.

A second assumption to be made in the following discussion is that the system is classical, as opposed to a quantum system. Since the characteristic electron energy in this work is 1 electron volt, the Landau level quantum number is of the order of 2×10^4, so quantum effects in the degrees of freedom transverse to the magnetic field can be ignored. Also, in view of the macroscopic size of the plasma (~10 cm) the velocity component parallel to the magnetic field can be considered continuous. The typical electron densities used in this work were around $10^9\ \mathrm{cm}^{-3}$. At this density, the Fermi energy corresponds to 10^{-3} degrees, so for a room-temperature plasma we certainly may neglect degeneracy effects.

B. Interaction

By considering the electron distribution in velocity space, one can write the equation of motion for an electron in a static magnetic field, $\vec{H} = H\hat{z}$, and a time varying electric field, $E(t)$:

$$\dot{\vec{v}} = \frac{-e}{m}\,\vec{E}\,(t) + \omega\,\hat{z} \times \vec{v}\,, \tag{1}$$

where ω is the cyclotron frequency. ($\omega = eH/mc.$) For the vector components transverse to the magnetic field we shall use the complex notation $v_x = \mathrm{Re}(\tilde{v})$ and $v_y = \mathrm{Im}(\tilde{v})$. In this notation, the transverse part of Eq. (1) becomes

$$\frac{d\tilde{v}}{dt} = -\frac{e}{m}\,\tilde{E}\,(t) + i\omega\tilde{v} \tag{2}$$

which is solved by the convolution

$$\tilde{v}(\omega,t) = \int_{-\infty}^{t} -\frac{e}{m}\,\tilde{E}(\tau)e^{i\omega(t-\tau)}\,d\tau\ . \tag{3}$$

The case of interest in this work is that of an electric field oscillating at a frequency near the cyclotron frequency and polarized linearly in a direction perpendicular to the magnetic field. Thus,

$$\tilde{E}(t) = \frac{1}{2}\,(E(t)\,e^{i\omega_o t} + E(t)\,e^{-i\omega_o t})$$

where $E(t)$ is real. Further, the assumption is made that $E(t)$ varies slowly compared with the oscillation frequency:

$$\frac{1}{E}\,\frac{dE}{dt} \ll \omega_0\ . \tag{4}$$

Then for times after the end of a microwave pulse,

$$\begin{aligned}\tilde{v}(\omega,t) &= -\frac{e}{m}\,e^{i\omega t}\,\frac{1}{2}\int_{-\infty}^{\infty}(E(\tau)e^{-i(\omega-\omega_o)\tau} \\ &\qquad + E(\tau)e^{-i(\omega+\omega_o)\tau})d\tau \\ &\approx -\frac{1}{2}\,e^{i\omega t}\,\frac{e}{m}\,E(\Omega)\ ,\end{aligned} \tag{5}$$

where $E(\Omega)$ is the Fourier transform of $E(t)$, and $\Omega = \omega-\omega_0$. If further we go to a frame rotating about $\vec{H}$ at frequency ω_0, then

$$\tilde{v}(\Omega,t) = -e^{i\Omega t} \frac{1}{2} \frac{e}{m} E(\Omega) \ . \tag{6}$$

Thus, the magnitude of the velocity of an electron with a particular cyclotron frequency will be proportional to the Fourier component at that frequency of the microwave pulse spectrum. Hereafter we shall refer to $\frac{1}{2}E(\Omega)$ as the area of the pulse.

For the simple model of two-pulse echoes the pulses will be assumed short enough so that $t_p \ll \Delta\Omega$, where t_p is the pulse width and $\Delta\Omega$ is the total electron spectral line-width. In this case the pulse spectrum is constant over the electron line, and the $e^{i\Omega t}$ term can be neglected during the pulse, so all the electrons respond identically. If the pulse spectrum is not constant over the electron line, it is possible, in view of Eq. (6) to store the spectral information in the electron velocity distribution. Harp, et al.[20] have shown this to be the case, and also they have shown that under suitable conditions this spectral information can be retrieved as modulation in the echo shape.

In this rotating frame in velocity space representation, the free motion of an electron is simply described by

$$\tilde{v}(t) = e^{i\Omega t} \, \tilde{v}(0) \ . \tag{7}$$

C. Simple Model

Using Eqs. (6) and (7) one can see what the response of the electrons will be to two pulses of resonant microwaves. The first pulse is applied at $t = 0$, and the second pulse, equal in area, is applied at $t = \tau$, where τ is much greater than the reciprocal spectral width of the electron resonance. As is shown in Fig. 2, the electron distribution in velocity space will be a thermal ball at $t = 0$ with a radius of about 0.17 $(\text{e.v.})^{1/2}$, corresponding to a Maxwell-Boltzman distribution at 300°K. After the first pulse the ball is displaced by v_0(~ 1 $(\text{e.v.})^{1/2}$). At $t = \tau$ the ball has fanned out into a doughnut, of radius v_0, due to the spread in Ω. The second pulse further accelerates those electrons that are in phase with the microwave pulse at $t = \tau$, and decelerates those that are out of phase with the pulse, resulting in a displaced doughnut after the second pulse. In fact, a simple geometrical construction shows that the velocity of any electron after the second pulse is given by

$$|\tilde{v}(\Omega)| = 2v_0 \left|\cos \frac{\Omega\tau}{2}\right| \quad . \tag{8}$$

This function is seen to be periodic in Ω with period $2\pi/\tau$. Since the radiating dipole moment is proportional to $|\tilde{v}|$, this velocity distribution in itself hints at beating, with beats spaced by τ in the time domain. However, care must be taken in considering the initial phases of the electron oscillators.

In order to see that no beating or echo phenomena occur for the system so far described, consider the classical cyclotron radiation from the electron gas. The dipole moment for a given oscillating electron is simply $-|e|R_c$, where R_c is the cyclotron radius. Since $R_c = v/\omega_c$, the electric dipole moment for an electron with cyclotron frequency ω_c

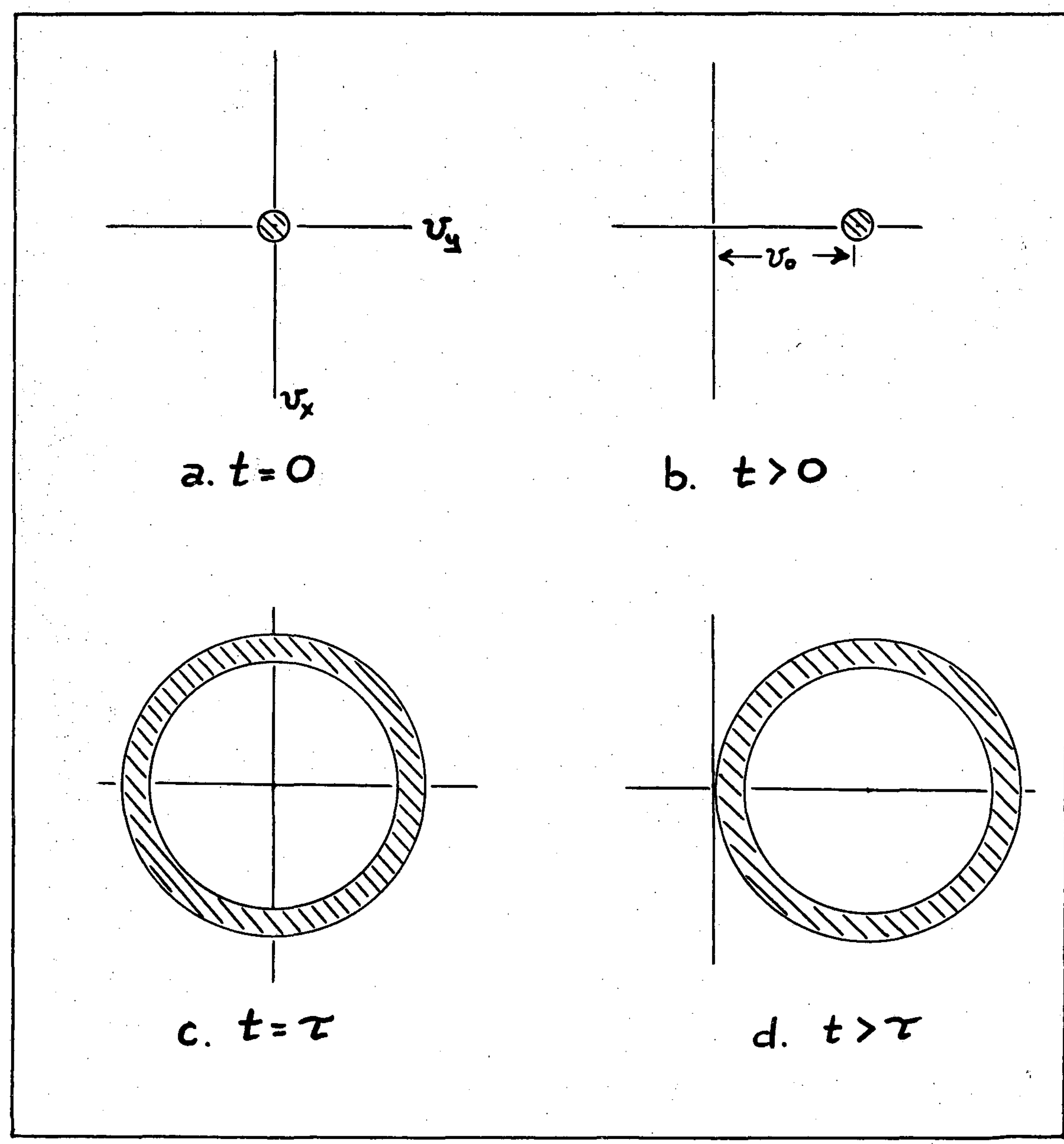

Figure 2. Electron velocity distribution at various times during the pulse sequence.

is $|\vec{p}| = \frac{mc}{H} |\tilde{v}|$. We can then define an average polarization for the whole gas as

$$\tilde{P}(t) = \int_{-\infty}^{\infty} \tilde{v}(\Omega,t)\; g(\Omega,t)\; d\Omega \;, \tag{9}$$

where we have gone to the complex notation in the rotating velocity space, and we have introduced an electron spectral distribution function, $g(\Omega,t)$, which may be time dependent. The distribution function is normalized so that $\int_{-\infty}^{\infty} g(\Omega,0)\, d\Omega = 1$. This form ignores propagation effects, and thus really applies only if the system is small compared with a microwave wavelength. The propagation effects will be considered in Section IIE. The total power radiated by a collection of coherently oscillating dipoles is

$$P = \frac{\omega^4}{3c^3} |N\vec{p}|^2 \quad , \tag{10}$$

where ω is the frequency, c is the velocity of light, and N is the number of oscillators. Therefore, the power radiated by the plasma electrons can be written

$$P = \frac{N^2 e^2 \omega^2}{3c^2} |\tilde{P}|^2 \quad . \tag{11}$$

This expression has, of course, ignored the incoherent dipole radiation which occurs even when $\tilde{P} = 0$. But the incoherently radiated power is less intense by a factor of N. That is, the power radiated incoherently by 10^{11} electrons (10^9 cm^{-3} over 10^2 cm^3 volume) is about 2×10^{-11} watts, or a factor of ten smaller than the sensitivity of the wide-band receivers used in this work.

Using Eq. (9), we can now calculate the linear response of the electron gas to resonant radiation pulses. Referring to Fig. 2, we can write

$$\tilde{v}(\Omega,0) = 0 \ ,$$
$$\tilde{v}(\Omega,t > t_p) = v_0 \ e^{i\Omega t}, \text{ and} \qquad (12)$$
$$\tilde{v}(\Omega,t > \tau + t_p) = v_0(e^{i\Omega t} + 1) \ e^{i\Omega(t-\tau)} \ .$$

Therefore,

$$\tilde{P}\ (0) = 0, \qquad (13a)$$
$$\tilde{P}\ (t_p < t < \tau) = v_0 \ G(t), \text{ and} \qquad (13b)$$
$$\tilde{P}\ (t > \tau + t_p) = v_0 \ (G(t) + G(t-\tau)), \qquad (13c)$$

where G (t) is the Fourier transform of the distribution function:

$$G(t) = \int_{-\infty}^{\infty} g(\Omega) e^{i\Omega t} \, d\Omega \quad .$$

These expressions have ignored the thermal smearing of the electron velocity distribution. Equation (13b) expresses the result, familiar as free induction decay in magnetic resonance,[22] that the response of a system to a delta function excitation pulse is just the Fourier transform of the system's spectrum. Since we have assumed that the electron spectral width is much greater than $1/\tau$, $g(t)$ is essentially zero for $t \gtrsim \tau$. Equation (13c) then shows that the response following the second pulse is simply another free induction decay, this time centered about $t = \tau$, the time of the second pulse. As promised above, there is no echo at $t = 2\tau$, or any later time.

From Fig. 2 we can see that the velocity of a particular isochromat has in general an x component after the second pulse. Therefore, at $t=\tau$, just after the second pulse, each isochromat has a phase , θ, associated with it, where $\theta = \tan^{-1}(v_x/v_y)$. If this phase is ignored, and the total velocity given by Eq. (8) is considered to be v_y at $t=\tau$ ($v_x = 0$ at $t=\tau$), then $(\tilde{v}(\Omega,\tau) = |\tilde{v}(\Omega,\tau)| = 2v_0|\cos\frac{\Omega\tau}{2}|$. Since this expression for $\tilde{v}$ is periodic in Ω and even, we can write it as a Fourier series:

$$\tilde{v}(\Omega,\tau) = v_0 \sum_0^\infty a_n[e^{in\Omega\tau} + e^{-in\Omega\tau}] \quad .$$

Then, inserting this into Eq. (9), we have the result:

$$\tilde{P}(t > \tau + t_p) = v_0 \sum_0^\infty a_n\{G(t + (n-1)\tau) + G(t-(n+1)\tau)\}, \qquad (14)$$

where the first few Fourier coefficients, a_n, are:

$$a_0 = 4/\pi$$
$$a_1 = \frac{1}{3}(4/\pi)$$
$$a_2 = -\frac{1}{15}(4/\pi)$$
$$\cdots \quad .$$

Thus we see maxima in the average macroscopic polarization centered around $t = (n+1)\tau$ for $n = 0, 1, 2, \ldots$. These maxima, echoes or beats, are just what one would expect from a spectrum of oscillators with amplitudes a periodic function in the frequency domain, if all the oscillators started out in phase. The importance of considering the phase of each oscillator exactly, is then clear, since the treatment of Eq. (12) leads to no response after the free induction tail following the second pulse. Thus, as expected, the linear system so far described behaves linearly.

The non-linearity we shall introduce in the simple model is the energy dependence of the elastic scattering cross section for electron-atom collisions.[19] This choice is motivated by the fact that the experimentally observed cyclotron echoes have maximum amplitudes for pulse spacings of the same order as the electron-atom collision times. The electron-Cs and the electron-A total scattering cross sections are shown in Fig. 3, along with an idealized cross section which is useful in conceptualizing

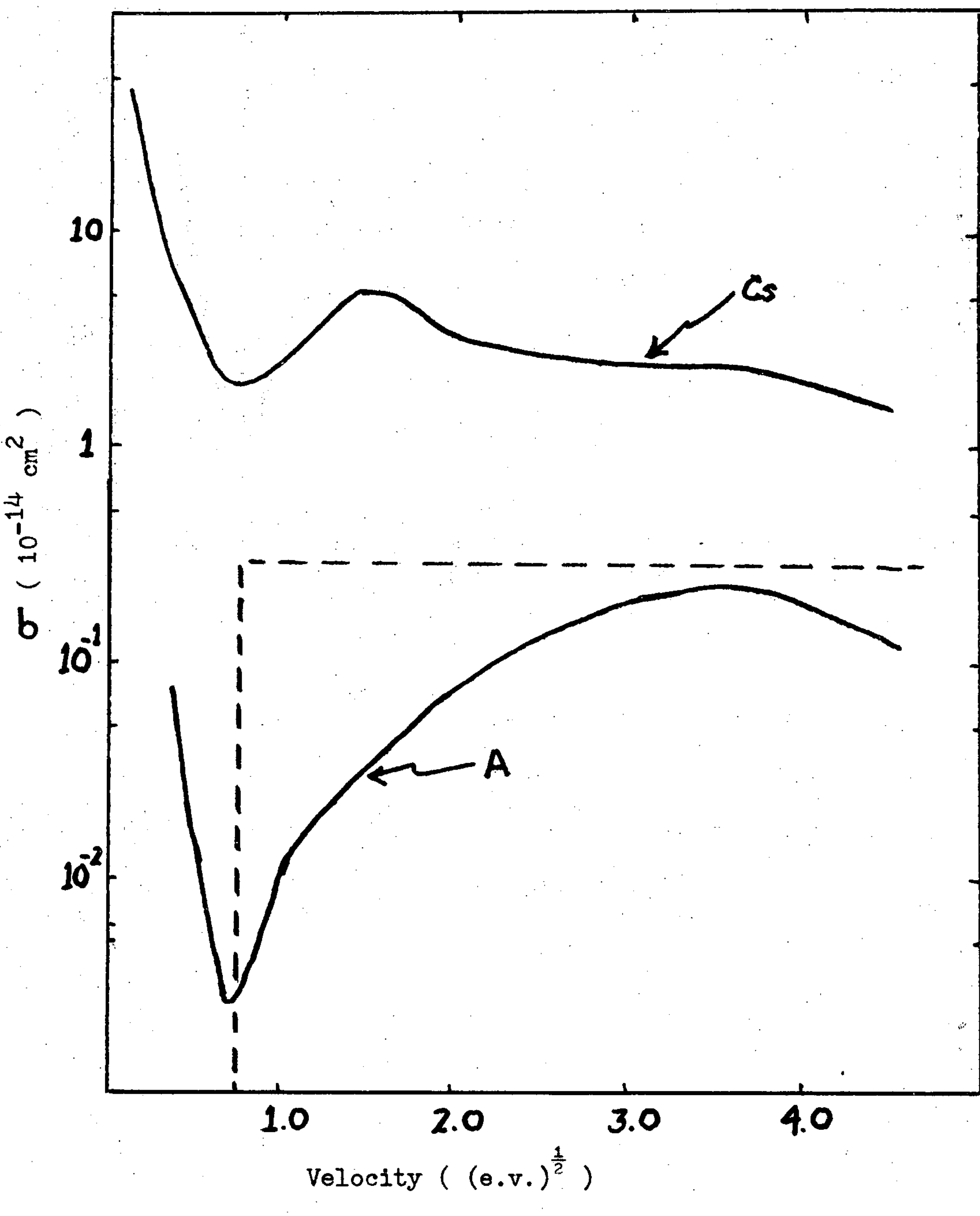

Figure 3. Argon and cesium total scattering cross sections as a function of electron velocity. The argon data and the cesium data above 0.5 (e.v.)$^{\frac{1}{2}}$ is from Brode[23], and the low energy Cs data is from Chen and Raether[24].

the echo process. The striking minimum in the Argon cross section is known as a Ramsauer minimum after the early measurements of this effect by Ramsauer.[25] This effect was explained theoretically by Allis and Morse,[26] who used the then new quantum mechanics of atoms. The effect arises essentially because an electron in the vicinity of a neutral atom polarizes it, thereby creating a potential well for the free electron. If the electron's de Broglie wavelength is comparable to the width of the potential well, then there is a possibility of resonant transmission through the well or reflection from the well. Allis and Morse's calculations indicated that this process was exactly what happened for electron energies in the one volt region, with the resulting large oscillation in the elastic scattering cross-section for electron velocities of about 1 $(e.v.)^{1/2}$. In the Cs case the measured cross-section is not entirely due to elastic scattering. The cesium D lines fall at 11,178 and 11,732 cm^{-1} respectively,[27] corresponding to an energy of 1.3 e.v. Thus, the cross-section measured around the peak at 1.5 $(e.v.)^{1/2}$ is for a combination of elastic and inelastic scattering events. This problem of interpretation does not arise in the Argon case, since the first excitation for Argon is at much higher energies than those used in this work.

The final step in the simple model is to include the effect of collisions on the distribution function. At any given time the electron in its orbit has a phase angle associated with it determined by the direction of the radius vector to the electron position relative to some fixed direction. This phase angle can be thought of as the angle between the instantaneous velocity vector and some arbitrarily defined direction perpendicular to the magnetic field. If the magnetic field variation is small over distances comparable to the cyclotron orbit size, electrons in orbits nearby the one under consideration will have essentially the same phase angle, if they are still oscillating coherently. Any change in this phase angle changes the phase of the radiated electric field, and only that component of the electric field in the direction of the radiated field from the unscattered electrons will add coherently to the radiation from the electrons. Such a change in the phase angle of an electron orbit is analogous to the T_2 processes of magnetic resonance. But an elastic scattering event results in just such a discontinuous change in phase angle. As a result of a scattering event, the electron velocity changes abruptly as the electron starts orbiting around a new center. The center of the orbit moves less than twice the cyclotron radius, so the fixed reference direction for determining phases is the same for the new orbit, while the direction of the radius vector changes abruptly. We shall defer until the next section a detailed discussion of what cross section is to be used in describing the relaxation of the polarization. For the simple model it suffices to say that we can separate the distribution function into a coherent part, g_c, for those electrons which have not been scattered, and an incoherent part, g_i, for those electrons which have been scattered.

$$g(\Omega,t) \equiv g_c(\Omega,t) + g_i(\Omega,t). \tag{15}$$

Since those electrons contributing to g_i have a random phase, the integration giving the macroscopic polarization will vanish for this part of the distribution function. Thus, only the coherent part of the distribution function is then to be used in Eq. (9) to calculate the polarization. The equation of motion for g_c can be written

$$\dot{g}_c(\Omega,t) = -\nu_c(\Omega,t)\, g_c(\Omega,t), \tag{16}$$

where $\nu_c(\Omega,t)$ is the collision frequency,

$$\nu_c(\Omega,t) = N\sigma(\Omega,t)\, v \quad , \tag{17}$$

where N is the density of scattering centers (e.g. neutral atoms), σ is a scattering cross section, which depends on Ω through the velocity dependence on Ω, and v is essentially the electronic velocity (or more precisely, the average relative velocity between the electron and an atom). Solving Eq. (16),

$$g_c(\Omega,t) = g_c(\Omega,0)\, e^{-\int_0^t \nu_c(\Omega,t')\,dt'} \tag{17}$$

one can see that the distribution function gets a periodic modulation imposed on it, since ν_c is now a periodic function of Ω. Therefore, one can see that the cancellation which resulted in no echoes in Eq. (13) no longer holds, and multiple echoes are expected. In fact, using the cross section model of Fig. 3, where

$$\sigma = \begin{cases} 0 & v < v_c \\ \sigma_0 & v > v_c \end{cases} ,$$

one can see that the fast electrons (those with frequencies around $\Omega = 0 \pm 2\pi n/\tau$) are rapidly scattered. The resulting distribution function is a relatively smooth one with periodic holes chewed in it spaced by $2\pi/\tau$. The resulting response should be that from the smooth distribution (free-induction decay) minus that from a distribution of oscillators spaced periodically in the frequency domain. The latter distribution gives pulses spaced by τ in the time domain in view of the fact that all those oscillators started almost in phase at $t=\tau$. A more accurate expression for an arbitrary cross section is derived in the next section.

D. Exact Description

We wish to derive the analog of Eq. (13c) with collisions included. After the first pulse, all the electrons have the same speed, so the collision time has no frequency dependence. Thus,

$$\begin{aligned} \tilde{P}(t_p < t < \tau) &= v_0 \int_{-\infty}^{\infty} g(\Omega,0)\, e^{-\int_0^t \nu_0\, dt'} \times (e^{i\Omega t}\, d\Omega) \\ &= v_0\, e^{-\nu_0 t}\, G(t) \, , \end{aligned} \tag{18}$$

where $g_c(\Omega,0) = g(\Omega,0)$, and ν_0 is the collision time associated with the electron speed v_0. After the second pulse the polarization is given by

$$P(t > \tau + t_p) = v_0\, e^{-\nu_0\tau}$$

$$\times \int_{-\infty}^{\infty} \left\{ (e^{i\Omega\tau} + 1)\; e^{-\int_\tau^t \nu_c(\Omega)\, dt'} \right\} \tag{19}$$

$$\times\; e^{i\Omega(t-\tau)}\, g(\Omega,0)\, d\Omega.$$

In this expression, both pulses have been assumed to have equal amplitude.

Since $|\tilde{v}|$ is a periodic function of Ω [Eq. (8)], so is $\nu_c(\Omega)$. Therefore, the term in braces in Eq. (19) is a periodic function of Ω, with period $2\pi/\tau$. We may then write

$$(e^{i\Omega\tau}+1)\, e^{-\nu_c(\Omega)(t-\tau)}$$

$$= \sum_{-\infty}^{\infty} a_n(t)\, e^{-in\Omega\tau} \tag{20}$$

where

$$a_n(t) = \frac{\tau}{2\pi} \int_{-\pi/\tau}^{\pi/\tau} e^{+in\Omega\tau}\, (e^{i\Omega\tau}+1)\, e^{-\nu_c(\Omega)(t-\tau)}\, d\Omega \tag{21}$$

Putting Eq. (20) back into Eq. (19), we have,

$$\tilde{P}(t > \tau+t_p) = v_0 e^{-\nu_0 t} \sum_{-\infty}^{\infty} a_n(t)\;\; G(t-(n+1)\tau). \tag{22}$$

Thus, the calculation of the nth echo amplitude has been reduced to the evaluation of the Fourier coefficient $a_n(t)$. Since $G(t-(n+1)\tau)$ is strongly peaked at $t = (n+1)\tau$, only $a_n((n+1)\tau)$ need be calculated.

Next we must come to grips with the problem of which cross-section to use. Unfortunately, there is no simple answer to this problem. If the electronic motion were confined to a plane, the answer would be that the momentum change cross-section should be used. Reference to Fig. 4 shows that in this case the phase shift, ϕ, in the electronic orbit is equal to the scattering angle, θ. The radiated electric field from such an electron still has a projection in the direction of the field radiated by the unscattered electrons, but it is reduced by a factor of cos θ by the scattering. That is, small angle scattering is not a very effective relaxation process. Therefore, the relevant cross section is just the momentum change cross-section, which weights events by a (1-cos θ) factor:

$$\sigma_m = \int (1-\cos\theta)\ d\sigma/d\Omega \quad d\Omega\ . \tag{23}$$

In Appendix A we prove that the above conclusion is valid even if scattering out of the plane transverse to $\vec{H}$ and into helical orbits is allowed if the magnitude of the magnetic field is constant along a flux line.

Experimentally, there are two problems which cast doubt on the accuracy of the model so far described. First, the magnetic field is not constant along a flux line. In fact, along a flux line $\Omega\tau$ for typical τ (200 nsec) varied through several π from one end of the plasma to the other. Using a model inhomogeneity, the effect of this complication could, in principle, be calculated in much the same way as diffusion in an inhomogeneous field was handled in Hahn's original paper.[3] However since $\Omega\tau$ varies by many π along a single flux line, there will be several places where $\Omega\tau = 2\pi n$ where n is an integer. Since these are regions where the electrons have large velocity and large scattering cross-sections,

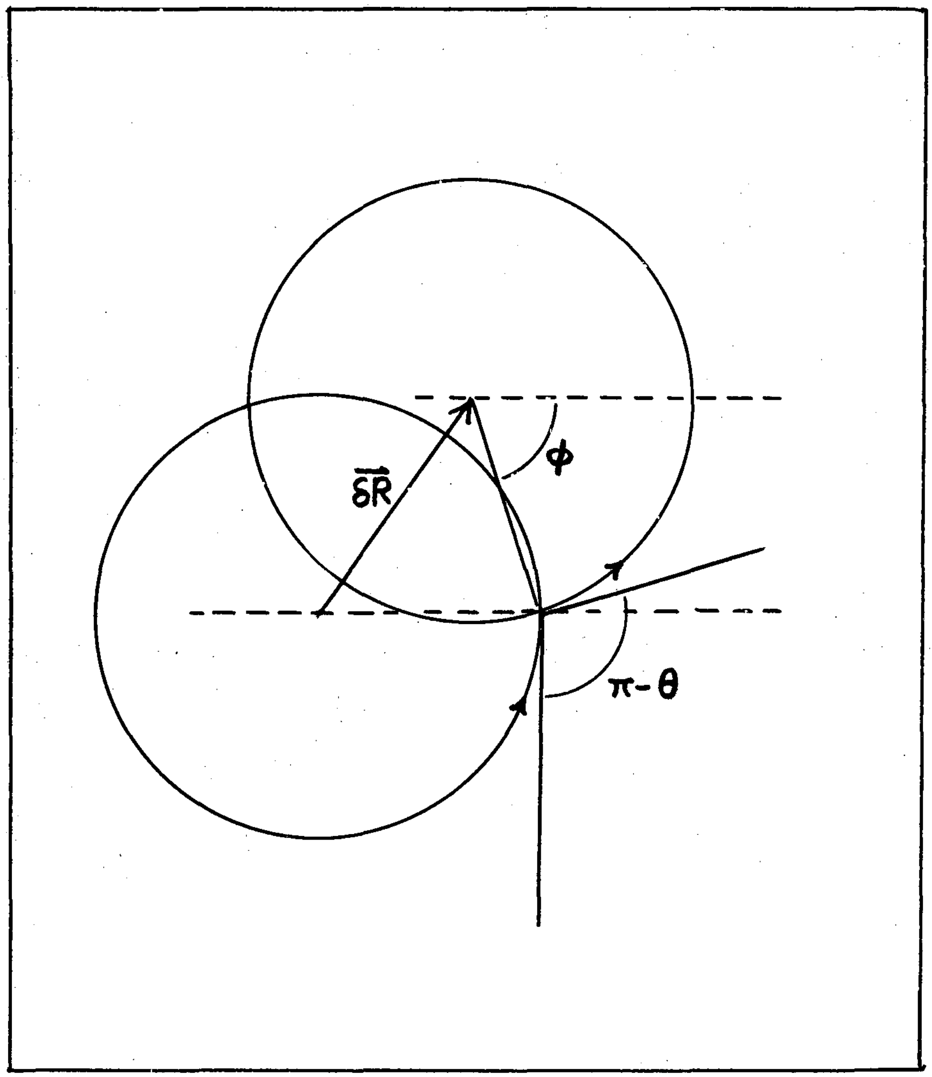

Figure 4. Effect of an elastic scattering on an electron orbit. Theta is the scattering angle; phi is the phase shift in the orbit; and $\vec{\delta R}$ is the change in the orbit center.

scattering in these regions is more rapid than in the intermediate regions. The result will be some space-charge developed along a flux line, and this is the second complication. If there are space charge fields along a flux line the motion of the electrons is no longer free in this direction. Then the complicated dynamics of an electron in the regime of ambipolar diffusion must be considered. More will be said about this complicated situation in reference to the three-pulse echoes.

In the case of a Cesium plasma, since the first excitation of the Cs atoms occurs at such low energies, inelastic collisions must be considered. We shall treat an inelastic collision in two parts. First, the velocity for an electron with an energy in excess of the excitation threshold is reduced to $(v-\Delta)$, where Δ is the electron velocity corresponding to the atomic excitation energy. Secondly, the electron is elastically scattered. From the calculation analogous to that already presented in Appendix A, we have then a new cross-section,

$$\sigma_i = \int [1 - (1- \frac{\Delta}{v}) \cos \theta] \left.\frac{d\sigma}{d\Omega}\right._i d\Omega \quad , \tag{24}$$

where $(d\sigma/d\Omega)_i$ is the inelastic differential cross section, which may still have a velocity dependence. This form was chosen since the weighting factor in square brackets is just $(P-P')/P$, where P' is the component of the scattered electron's polarization along the direction of the unscattered electronic polarization. P is the polarization of a single electron before scattering. If Δ goes to zero in Eq. (24), σ_i goes to σ_m, which is correct since the scattering becomes elastic. If $v = \Delta$, σ_i becomes the total inelastic cross section since any scattering event will cause the electron velocity to vanish, and in such a case every inelastic scattering event is completely successful at destroying the radiation from the electron involved. The cross section to be used in the collision frequency of Eq. (21), if there is no variation in magnetic field along a flux line, is then

$$\sigma = \sigma_m + \sum_n \int \left[1 - \left(1 - \frac{\Delta_n}{v}\right) \cos\theta\right]\left(\frac{d\sigma_n}{d\,\Omega}\right)_i d\Omega \qquad (25)$$

where σ_m is the elastic scattering momentum change cross section, and the sum is over final atomic states for an inelastic process.

In order to simplify the expression (25), we shall replace the sum with the total inelastic cross section. Since in the experiments described in this report the electronic velocity is never more than twice the first inelastic threshold, calling the sum the total inelastic cross section is at least a better approximation than calling it the momentum change inelastic cross section. However, Brode's data,[23] shown in Fig. 2 are for the total elastic, σ_e, plus the total inelastic cross sections.

Some measurements have been made,[28] by a crossed beam technique, of the differential scattering cross-section for electron-potassium collisions. These measurements indicate a considerable increase in small angle scattering as the electron velocity is increased. Also, data presented by Brown,[29] show σ_m for e^--A and e^--Ne collisions falling below the total elastic cross sections. The difference between σ_m and σ_e in these rare-gas cases appears to be linear in electron energy up to about 10 e.v. If the Cs cross-section data were for purely elastic scattering, we could simply assume a similar scaling law held in Cs and multiply Brode's data by $(1-xv^2)$ where x would be a variable parameter chosen to fit the data, and v is the electron velocity. However, calculations by Karule and

Peterkop[30] indicate an inelastic contribution to the total cross section which rises to 50% for electron energies of 5 volts. In view of the decreasing contribution of elastic scattering to the total cross section and our approximation of using the total inelastic cross-section in Eq. (25), a more accurate fudge factor with which to multiply Brode's data would be (1-xv).

Computer calculations of the two pulse echo amplitudes, $e^{-v_0\tau} a_n(n+1)$ as given by Eq. (21) will be presented shortly. First, some exact results proved in Appendix B will be discussed. The first results proved are that for the velocity dependent collision frequency mechanism, the echo amplitude is linear in τ for $\nu_c\tau \ll 1$, and the echo amplitude is zero if the collision frequency is independent of velocity. Obviously these results are just statements of the facts that one needs collisions before echoes appear, and that the collisions must affect different parts of the spectrum differently. Next, if the collision frequency is a monotonic increasing or a monotonic decreasing function of velocity, and the area of the first pulse is less than or equal to the area of the second pulse, the power of the first echo has a single maximum. If the area of the first pulse is greater than the area of the second pulse, there may be more than one maximum. If one ignores the low velocity increase in σ shown in Fig. 3, (this is less pronounced in ν_c since $\nu_c \propto v\sigma$), one sees that the electron-atom collisions give a monotonic increasing $\nu_c(v)$. If electron-ion collisions are the dominant process, the collision frequency is a monotonic decreasing function of velocity ($\nu_c \propto 1/v^3$).[31] The conclusion is that unless one can measure the phase of the echo relative to the input pulses, there is no way of distinguishing a monotonic increasing $\nu_c(v)$ from a monotonic decreasing one.

These general conclusions have been verified by Herrmann, et al.[13] They performed numerical calculations of the echo power as a function of τ for $\nu_c \propto v^2$ and $\nu_c \propto 1/v^3$, approximations to the electron-atom and electron-ion collision frequencies, respectively. They found, as we have shown in general, that for $v_1 \leq v_2$, there is a single maximum in the echo envelope, and for $v_1 > v_2$ there may be multiple maxima.

Lastly, it is proven in Appendix B that if the collision frequency is not a monotonic function of velocity, then under suitable conditions the amplitude of the first echo can pass through zero. In particular, for

$$\nu_c = \begin{cases} b & v < v_2 \\ a & v_2 < v < v_1 \\ c & v > v_1 \end{cases} \quad , \tag{26}$$

where $v_1 > v_2$, if $b < c < a$, and if c is small enough, $a_1(2\tau,\tau)$ changes sign for a τ denoted τ_c. This critical τ shows up in the echo envelope as that τ for which the echo power goes to zero. For a given c, τ_c varies in an involved way as the input pulse area is increased above a certain threshold. At this threshold, τ_c is zero, and below the threshold, there is no τ_c. Also, for a given pulse area above threshold, τ_c is roughly proportional to c^{-1}. That is, as c is decreased, τ_c moves away from zero.

The relevance of these analytical results can be appreciated by referring to Figs. 3 and B2. It is seen that the model looks very much like the actual e^- - Cs collision frequency. Then, since the corrections discussed in relation to reducing the elastic scattering component in Brode's data tend to reduce the collision frequency at high velocities (c), one expects the echo power to be zero for some τ, and this critical τ should behave roughly as predicted by the results of Appendix B.

The computed echo power as a function of τ, and input pulse area (v_0), for Brode's cross section is shown in Fig. 5. The quantity labelled power is given by

$$\text{power} = \left(e^{-\nu_0\tau} \; a_n\left((n+1)\tau,\tau\right)\right)^2 , \tag{27}$$

where n is the echo number.
The calculation was performed by a Simpson's Rule integration of Eq. (21) with one hundred intervals between $\Omega\tau = 0$ and $\Omega\tau = \pi$. These curves correspond to a Cs pressure of 10^{-4} torr, but a change in pressure only results in a scaling of τ. That is, since the Cs pressure enters the calculation only through ν_c, and since ν_c appears only in the expression ($\nu_c\tau$), doubling the Cs density has the same effect as scaling τ up by a factor of two. The units for v_0, the velocity corresponding to the input pulse area, are $(\text{e.v.})^{1/2}$. These curves are compared with the experimental data in Chapter IV with quite satisfactory agreement.

Similar curves were computed using the σ shown in Fig. 3, multiplied by (1-xv). For x large enough (0.13), τ_c became non-zero, and the echo envelope assumed the appearance of that shown in Fig. B3. The variation of τ_c with v_0 and x is shown in Fig. 6. The scale on τ_c again corresponds to a Cs pressure of 10^{-4} torr. Similar curves were obtained when the correction factor $(1\text{-}xv^2)$ was used. In fact, even had τ_c been observed experimentally, choosing between the two correction factors would not have been possible.

In order to search for τ_c, experiments were done with v_0 up to at least 1.3 $(\text{e.v.})^{1/2}$, but no τ_c was observed. One can then place an upper limit on x, if indeed this model is valid, of 0.15.

Two more complications in the simple model should be mentioned.

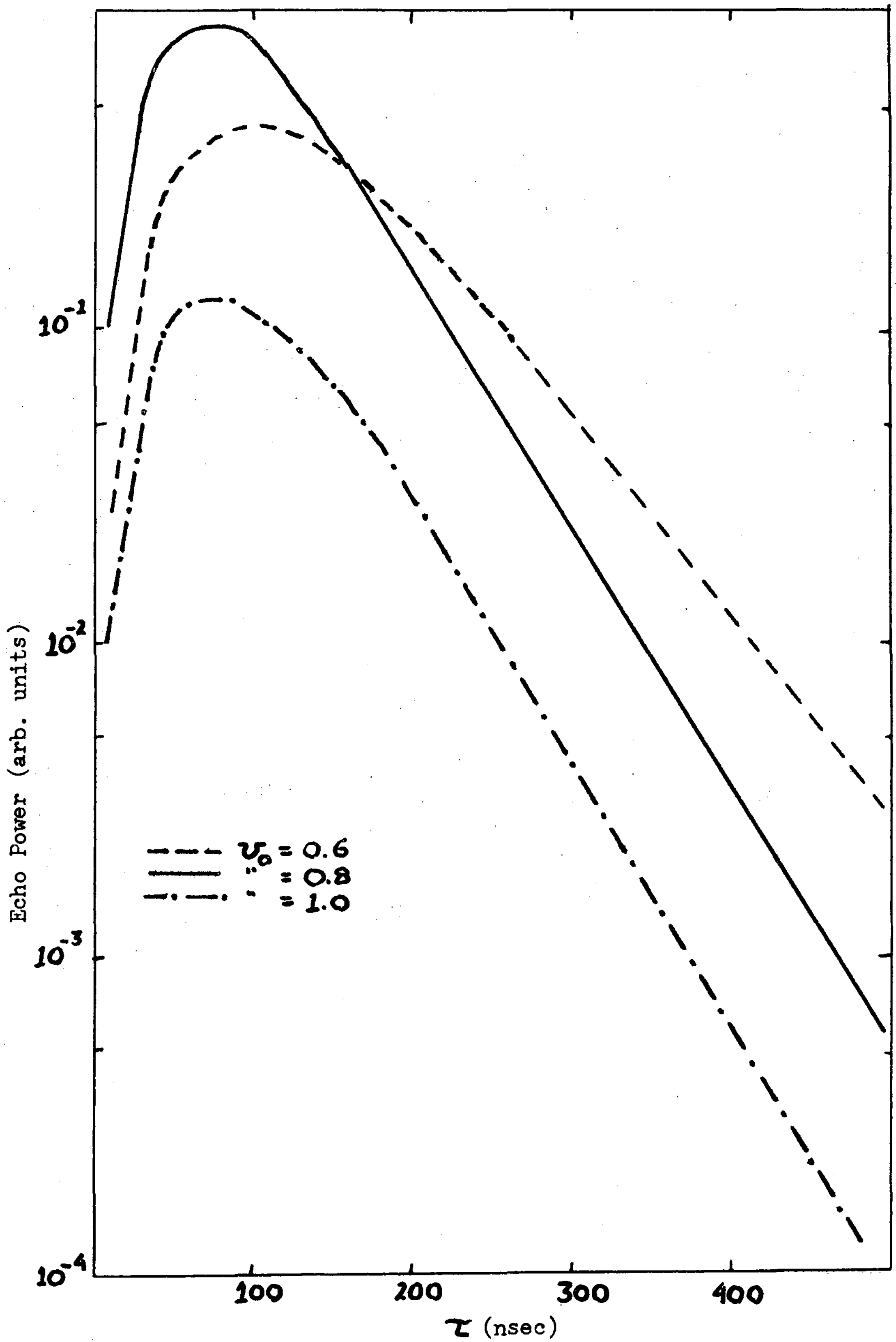

Figure 5. First two-pulse echo power calculated for Brode's uncorrected data.

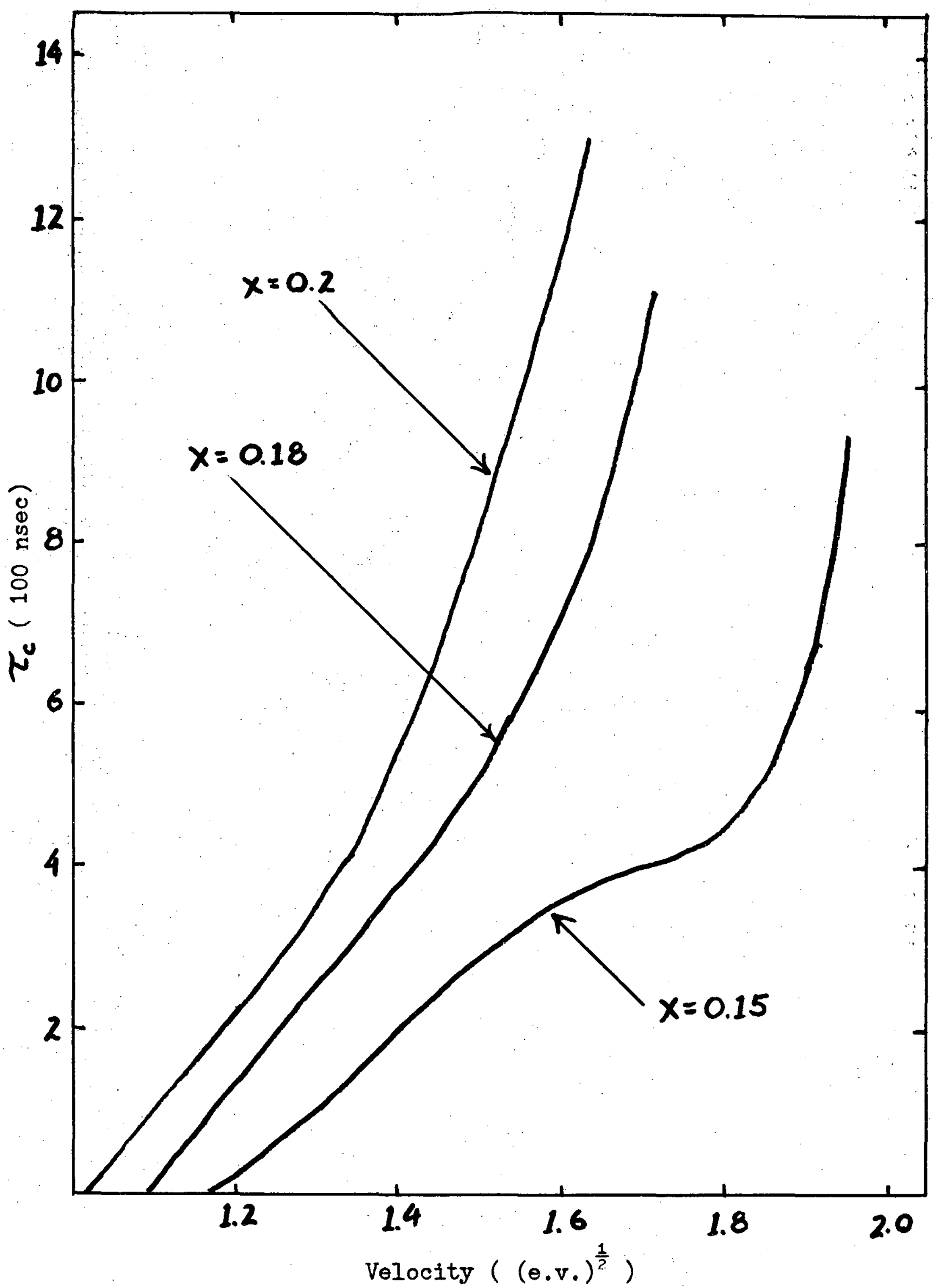

Figure 6. Calculated τ_c for Brode's cross section data multiplied by (1 - xv).

First, the calculations really should take into account the thermal smearing of the initial electron velocity distribution. Secondly, since the microwave electric field is not expected to be uniform across the whole sample, one should calculate an echo amplitude for a particular part of the microwave model, average over the mode, and then square the amplitude to get the echo power.

Numerical integrations for the echo power were performed with electron velocities before the first pulse averaged over circles of radius 0.1 and 0.4 $(e.v.)^{1/2}$. A uniform distribution was assumed over these circles. In the case of the 0.1 $(e.v.)^{1/2}$ radius circle, which was taken to approximate the Maxwell-Boltzman distribution for an electron temperature of 150°K, the calculated echo power nowhere deviated by more than 10% from the echo power calculated for an electron temperature of 0°K. The average over an 0.4 $(e.v.)^{1/2}$ circle was taken to approximate an electron temperature of 2000°K. Calculations for this case indicated an overall shift up or down of the echo envelope, depending on whether v_0 was less than or greater than that corresponding to a pulse area giving a maximum echo amplitude. In no case was the shift by more than a factor of two in power, and in every case the characteristic structure shown in Fig. 5 was preserved. Since the electron temperature was probably not much different than that of the ambient gas in the experiments (500°K), we assume that thermal averaging does not require significant changes in the curves shown in Fig. 5.

In the experiments reported here, the microwave power incident on the discharge bulb did not vary by more than 3db over the whole bulb. One or two db variations over the plasma volume would be a reasonable estimate. Since this implies a pulse area variation of less than 20%, an average over the microwave mode was not considered necessary. If the experiment were done in waveguide, such an average would certainly be in order.

If the thermal or mode averages are applied to the corrected Brode data, they result in a considerable shift in τ_c. However, they do not alter the characteristic cusp-like shape of the zero in echo power. When the possible 20% variation in input pulse area is taken into consideration, the upper limit on x in the correction factor raises to $x \leq 0.18$.

E. Potpourri

If one relieves the restriction of v/c being small, several new effects enter the problem,[17] the most interesting of which is the relativistic mass shift.[18,32] This problem can be treated as an example of an anharmonic oscillator. We write first

$$\omega_r \approx \omega\,(1 + v^2/2c^2) \quad , \tag{28}$$

for the relativistic frequency shift to lowest order, and

$$\alpha \equiv \partial^2\omega_r/\partial v^2 \approx \omega/c^2 \quad . \tag{29}$$

In this section, we shall not use the rotating velocity space, since the results are more straightforward in the standing-still velocity space. We write the velocity after a first pulse as

$$\tilde{v}(\omega,t) = v_1\, e^{i\omega' t} \tag{30}$$

where $\omega' = \omega + \frac{1}{2}\alpha\, v_1^{\,2}$, and $v_1 = -\frac{1}{2}\frac{e}{m}E(\omega)$. We shall assume, as usual, that the pulse width is much smaller than the electron spectral width, so v_1 is a constant independent of ω. If a second pulse is applied at $t = \tau$,

$$\tilde{v}(\omega, t > \tau) = (v_1 \, e^{i\omega'\tau} + v_2) \, e^{i\omega''(t-\tau)} \quad , \tag{31}$$

where $v_2 = -\frac{1}{2}\frac{e}{m} E_2(\omega')$, and

$$\omega'' = \omega + \frac{1}{2}\alpha \, (v_1^{\,2} + v_2^{\,2} + 2v_1 v_2 \cos \omega'\tau). \tag{32}$$

We must assume $E_2(\omega') = E_2(\omega)$ is uniform over the electron spectrum also, or else we get into the same problem the early cyclotron builders found. That is, as the mass shifts during a pulse, the gyrofrequencies of some oscillators will be shifted so far as to be unaffected by the remainder of the pulse. Thus, we still confine ourselves to small mass shifts. The polarization is now

$$\tilde{P} = \int_{-\infty}^{\infty} g(\omega) \, (v_1 e^{i\omega'\tau} + v_2) \, e^{i\omega''(t-\tau)} \, d\omega \quad . \tag{33}$$

We write[33]

$$e^{i\alpha v_1 v_2 (t-\tau)\cos\omega'\tau} = \sum_{-\infty}^{\infty} (-i)^n \, J_n(\beta) \, e^{-in\omega'\tau} \quad , \tag{34}$$

where $\beta = \alpha v_1 v_2 (t-\tau)$, and J_n is the Bessel function. Then note that $g(\omega)$ is a fairly sharply peaked function for the conditions already specified. In typical cyclotron echo experiments, the width of $g(\omega)$ is less than $0.01\,\omega$. Putting in typical numbers of 6×10^{10} sec^{-1} for ω, 10^{-7} sec for τ, 10^{8} cm/sec for v, $\alpha v^2 \tau \approx 0.06$. Thus, all terms involving $\exp(i\,\alpha v^2 (t-\tau))$ are essentially constant over the region where $g(\omega)$ is non-zero for t many times τ. Therefore, we may pull all such terms out of the integral and replace ω in them by ω_0, the center of the line. Then

$$\tilde{P} = \Sigma \quad a_n(t-\tau)\ G(t-n\tau) \quad , \tag{35}$$

where

$$a_n = e^{i\frac{1}{2}\alpha(v_1^{\,2}+v_2^{\,2})(t-\tau)}\ e^{i\frac{1}{2}\alpha v_1^{\,2}(1-n)\tau}$$
$$\times \left[(-i)^n J_n(\beta)\ v_1 + (-i)^{n-1} J_{n-1}(\beta)\ v_2\right] \tag{36}$$

This is essentially the result of Kegel and Gould,[18] but in the final approximation, they used the large argument expansion of the Bessel Functions. The numbers we have used show that the small argument expansion is more appropriate. Since the first echo occurs at $n = 2$, we expand the Bessel functions and find that to lowest order in v^2/c^2,

$$a_2 \approx (-1)v_2\ (\omega_0\tau)\ \frac{v_1v_2}{c^2} \quad . \tag{37}$$

Putting in the numbers quoted above, this expression gives an echo power one order of magnitude weaker than the maximum calculated echo for Cs and three orders of magnitude weaker than the maximum calculated echo for Argon. Of course, scattering will tend to reduce this echo amplitude. Higher order echoes have powers reduced by factors of $(v^2/c^2)^2$, so they would be more difficult to observe.

It can be seen that this mechanism would compete with the velocity dependent collision frequency for a relatively small increase in v. Also, in a semi-conductor where the conduction band may not be exactly parabolic, the effective mass shift will act just like the relativistic mass shift of a free electron. For example, it was shown by Aggarwal, et al.,[34] that in Ge the effective mass for cyclotron motion in a plane perpendicular to the long axis of the constant energy ellipsoids [(111 axis)] has an energy dependence:

$$m_\perp = m_\perp(0)\left(1 + \frac{2\Delta\epsilon}{\epsilon_g}\right) , \tag{38}$$

where $m_\perp(0)$ is the mass at the bottom of the conduction band, $\Delta\epsilon$ is the energy measured from the bottom of the conduction band, and ϵ_g is the band gap. Since $\epsilon_g = 0.67$ volts, it is easy to see that the mass shift is significant even for $\Delta\epsilon$ a small fraction of a volt. Unfortunately, to date no observations of cyclotron echoes in such a solid have been made because the scattering time is in general far too short ($\sim 10^{-12}$ sec).

If the plasma sample is comparable with the wavelength of the microwave radiation, but still small compared with an absorption length, then the direction of observation of the echo is of some importance. Cyclotron echoes have been observed in transmission and reflection, and these will be the two cases discussed. Two plane wave pulses propagating through the plasma will set up a polarization like that of Eq. (19), but with an additional spacial dependence:

$$P(x,t) \propto e^{i(kx-\omega t)} , \tag{39}$$

where x is measured from the surface where the radiation enters the plasma. We shall consider a rectangular plasma volume, so the problem is reduced to a one-dimensional one.

The radiation from the polarization at x arriving at point x' at time t can be written

$$E_r(|x'-x|,t) \propto e^{i[kx-\omega(t-\frac{|x'-x|}{c})]} . \tag{40}$$

Let the plasma extend to x = L. For forward scattering we calculate E_r for x' = L. Then,

$$E_r\,(L-x,t) \propto e^{i(kL-\omega t)} \quad , \tag{41}$$

which is independent of x. Thus all the radiation from the plasma adds in phase at the exit boundary, and the calculation is the same as that for plasma dimensions small compared to the wavelength.

In order to calculate the echo radiation in the reverse direction, let $x' = 0$. Then

$$E_r\,(x,t) \propto e^{i(2kx-\omega t)} \quad . \tag{42}$$

Integrating over the sample length,

$$E_r \propto e^{ikL}\, e^{-i\omega t} \left[\frac{\sin kL}{kL}\right] \quad . \tag{43}$$

Thus, the reverse radiated echo power is less than the forward radiated power by a factor of the square of the term in the brackets. Since the term in brackets oscillates, the reverse radiated power may be a sensitive function of k and the plasma dimensions. For the real plasma, however, the volume is more ellipsoidal, and there is some damping as the wave propagates. Both of these effects will smooth out the oscillations in the reverse radiated power. However, one would expect in general to get more echo power in the forward direction. Typically the difference experimentally measured is a factor of five.

Finally, if the plasma dimension is much larger than an absorption length the problem would have to be handled self-consistently, as was done for optical pulse propagation.[35]

F. Relation to Spin Echoes

Earlier in this chapter, we showed two systems with a periodic modulation of oscillator strengths in their spectra. One of these systems gave no echoes at all, and the other gave an infinite train of them. In Appendix C, we give a similar system - a spin 1/2 system in an inhomogeneous magnetic field. It is shown there that following two 90° pulses the transverse component of the spin, or magnetization also has a periodic modulation. This system gives one and only one echo, again due to the initial phasing of the oscillators. Any mechanism that alters the magnitude of the transverse spin, and that depends on the magnitude of the transverse spin, is analogous to the velocity dependent collision frequency for cyclotron echoes. This is proved in Appendix C. Thus, it is at least mathematically possible to generate multiple echoes from a collection of two level oscillators.

This observation is especially appropriate to the subject of photon echoes in ruby. Since an electric dipole transition is involved in these echoes, what we have written as the transverse spin corresponds to the total electric dipole moment. If the chromium density in the ruby is high enough, or if there is local clustering of chromium atoms, dipole-dipole coupling may become strong. The local electric field seen by one chromium atom will then be proportional to the dipole moments of its neighbors. If Ω is slowly varying over the nearest neighbor distance, then for pairs or for low symmetry clusters of chromium atoms, the local electric field of a chromium atom has a component rotating at the local resonant frequency and 90° out of phase with the instantaneous polarization. Such a local field has the same effect as a resonant pulse, but it will typically act over a longer time ($\tau > t_p$), and need not be so large to alter the angle of the chromium dipole.

To give an order of magnitude for this effect in ruby, we write

$$T_2 \approx \frac{1}{\omega_1} = \frac{\hbar}{pE_{loc}} = \frac{\hbar r^3}{p^2} \quad ,$$

where r^3 is the neighbor distance. For chromium pairs separated by 10Å in ruby, $T_2 \approx 10^{-8}$ sec. Since this number is not far from τ in typical photon echo experiments, and $r \approx 10$Å corresponds to 2% doped ruby without clustering, or much less with clustering, this mechanism should yield multiple photon echoes.

Multiple photon echoes have been observed by Abella, et al.[6] in Ruby, and by Bolger and Diels[7] in Cs vapor. Abella, et al. have attributed their multiple echoes to the echo radiation acting as a third driving pulse, and they reference two other observations of similar phenomena. However, in these two other observations the fields from the echoes had an artificial enhancement. In one case they were radiated into a high Q cavity.[36] In the other case nuclear spin echoes were observed in a ferromagnetic metal, where a small low frequency field drives the electron spins, thereby resulting in large resonant hyperfine fields acting back on the nuclei.[37] The echoes of Abella, et al. have no such field enhancement, and, judging from the published oscilloscope traces, they represent very small angle pulses. Their first echo appears to be 30db less intense than their transmitted pulses, which may be taken for 90° pulses. If this is the case the echo pulse acts as a 2° pulse, and the second echo should be another 60db less intense than the first. The oscilloscope trace in the paper by Abella, et al., indicates a second echo power more like 10 db below the first echo power. In view of these comments, it would be interesting to see a more complete calculation of multiple echoes and more experimental data on multiple echoes vs doping in ruby.

III. THREE-PULSE ECHOES

If a third microwave pulse is applied to the electron gas a time τ_3 after the second pulse, another train of echoes is generated. These echoes appear at $t = \tau + \tau_3 + n\tau$ where n is an integer (see Fig. 1). The initial observation[13] of these three pulse echoes showed that they persisted for τ_3 as large as tens of microseconds, a time long compared with the electron-neutral collision time, but short compared with the electron thermalization time. The power of the first three-pulse echo ($n=1$) as τ_3 is varied shows a non-monatonic structure,[13] and if τ_3 is kept fixed while τ is increased the power of this echo decreases rapidly.

One mechanism that explains the qualitative features of the three-pulse echoes is that presented by Harp, et al.[20] They considered a collision frequency similar to the model shown in Fig. 3. That is,

$$\nu_c(v) = \begin{cases} 0 & v < v_c \\ \nu_c & v > v_c . \end{cases}$$

Let the magnetic field be constant along the flux lines and have a linear inhomogeneity perpendicular to the flux lines. Then, for incident pulse areas large enough, after the second pulse the plasma volume will consist of slabs of hot electrons ($v > v_c$), alternating with slabs of cold electrons ($v < v_c$). Electrons in the cold slabs will stay pinned on their flux lines, while those in the hot slabs will tend to diffuse over the whole plasma volume. When the hot electrons have diffused half-way out into the low velocity slabs, we can say that those electrons for which $-\theta_c < \Omega\tau \pm 2\pi n < \theta_c$ ($\theta_c = \Omega\tau$ for which $v = v_c$ as in Eq. (8)), where n is an integer, have been redistributed uniformly over the whole spectrum. The result is again a periodic modulation of the spectrum. The phases have by now been randomized, so at the time of the third pulse, the net moment of each isochromat is zero. The third pulse excites the electrons uniformly, so the spectrum of oscillators, with periodic modulation in the spectral distribution function starts out in phase at $t = \tau + \tau_3$. Therefore, one expects an infinite train of beats, or echoes, spaced by τ in the time domain, as predicted in Eq. (14).

If we consider N electrons per unit length on a single flux line, and solve the two-dimensional diffusion equation for the concentration n,

$$\frac{\partial n}{\partial t} = D \nabla^2 n \tag{44}$$

where D is the diffusion coefficient,

$$n(r,t) = \frac{N}{4\pi Dt} e^{-r^2/4Dt} . \tag{45}$$

In this solution, r is the distance the center of the cyclotron orbit has moved. For diffusion of the orbit center across flux lines, the diffusion coefficient is given by[38]

$$D = \frac{(R_c)^2}{2t_c} , \tag{46}$$

where R_c is the cyclotron radius, and t_c is a collision time. Thus for diffusion to spread the line of electrons out over a distance, ℓ, we must have

$$t \approx \frac{\ell^2}{4D} .$$

Further, if we take the high and low velocity slabs as roughly equal in thickness, the spacial distance between them, L, will be

$$L = \frac{\pi mc}{e(dH/dx)\tau} . \tag{47}$$

Then the characteristic time for the redistribution of the hot electrons will be

$$T = \left[\frac{\pi}{1/H\ (dH/dx)}\right]^2 \times \frac{1}{2\langle v^2\rangle} \quad \frac{1}{\nu_c \tau^2} \quad . \tag{48}$$

The $\langle v^2 \rangle$ in the denominator of Eq. (48), is an average over the velocities of the hot electrons.

Two mechanisms will tend to damp out the spacial inhomogeneity in the electron density. These are space change effects and the non-zero collision frequency of the cold electrons. Any space charge fields in this model will be directed perpendicular to the slabs. Since the space change field is perpendicular also to the magnetic field, the result is that the electron orbit centers will drift parallel to the slabs and perpendicular to the electric and magnetic fields. This drift is seen to leave the spectral distribution function unchanged. If the magnetic field inhomogeneity is more realistic than the one chosen for the model, drift can alter the spectral distribution function. However, since the drift velocity is (E/H)c, where c is the speed of light, space charge fields in excess of 100 volts/cm would be required to cause the electron orbit center to drift significantly (several cm) in a microsecond. Also, since the surfaces of constant magnetic field at least near the center of the plasma bottle will be almost planar even for a real system, the space-charge fields will be approximately perpendicular to the constant field surfaces. Therefore, the drift is still confined roughly to constant field surfaces, as in the linear inhomogeneity case, and the electrons near the center of the plasma will not be significantly dephased by this drift.

If ν_c is non-zero for the cold electrons, there is a characteristic time for decay of the periodicity in the spectral diffusion function which is obtained from Eq. (48) by replacing ν_c by the cold electron collision frequency. In the real plasma, of course, the diffusion coefficient is a continuous function of electron velocity, making an exact calculation even for a model field inhomogeneity out of the question. If we put in typical numbers of 3000 gauss for H, 10 gauss/cm for dH/dx, 1.5×10^{8} cm/sec for $\langle v^2\rangle^{1/2}$, 2×10^{7} sec^{-1} for ν_c, and 2×10^{-7} sec for τ, we have that $T \approx 25$ μsec. The damping mechanisms will tend to make the peak of the three-pulse echo envelope occur at earlier times, in good rough agreement with the experimentally observed envelope. Also, as τ is increased, scattering between the first and second pulses will tend to randomize the velocities after the second pulse, thereby reducing the sharp spacial variation in electron velocity. This process then reduces the amplitude of the three pulse echo as τ is increased with a decay rate roughly equal to the decay rate of the two pulse echoes.

As an example of this model, we will calculate the magnitude of the electron spacial density modulation for the one dimensional system depicted in Fig. 7. This figure depicts the hot (n_1) and the cold (n_2) electron densities immediately after the second pulse. We assume diffusion coefficients, D_1 for the hot electrons, and D_2 for the cold electrons, where $D_1 > D_2$. We are only interested in the magnitude and time development of the electron density modulation, so we shall calculate $n(\Omega\tau,t) = n_1(\Omega\tau,t) + n_2(\Omega\tau,t)$ for $\Omega\tau = 0$ and $\Omega\tau = \pi$.

The solutions to the diffusion equations for this system are[41]

$$n_1(0,t) = n_1(0,0) \left\{ \operatorname{erf}\left(\frac{a}{4\sqrt{D_1 t}}\right) + \sum_{n=1}^{\infty} \left[\operatorname{erf}\left(\frac{(4n+1)a}{4\sqrt{D_1 t}}\right) - \operatorname{erf}\left(\frac{(4n-1)a}{4\sqrt{D_1 t}}\right) \right] \right\} \tag{49}$$

$$n_1(\pi,t) = n_1(0,0) \left\{ \sum_{n=1}^{\infty} \left[\operatorname{erf}\left(\frac{(4n-1)a}{4\sqrt{D_1 t}}\right) - \operatorname{erf}\left(\frac{(4n-3)a}{4\sqrt{D_1 t}}\right) \right] \right\}$$

where erf denotes the standard error function. Similar equations are obtained for n_2.

In Fig. 8 we plot $\alpha(t) = (n(\pi,t) - n(0,t))/n(0,0)$, which is just the degree of modulation in the spectral distribution function. D_1 was taken to be 625 cm^2/sec, $D_2 = 1/4\ D_1$, and a was taken as 0.1 cm, in accordance with the typical experimental numbers already presented.

If the modulation of the spectral distribution function were sinusoidal in Ω, we could write

$$g(\Omega,t) = g(\Omega,0)[1-\alpha(t)\cos\Omega\tau]. \tag{50}$$

Then the polarization after the third pulse (applied at $T' = \tau + \tau_3$) would be

$$p = \int_{-\infty}^{\infty} g(\Omega,t)\, e^{i\,(t-T')} = G(t-T') - \frac{1}{2}\alpha(t)\,[G(t-(T'+\tau)) + G(t-(T'-\tau))] \tag{51}$$

The first term in the bracket of Eq. (51) is an echo centered at $t = T'+\tau$, with amplitude $\frac{1}{2}\beta(t)$. Thus, as τ_3 is varied, this echo should map out the envelope specified by $\alpha(\tau_3)$. In general, the periodic modulation of $g(\Omega)$ has higher harmonic content, and the higher harmonics result in higher order echoes spaced τ apart in the time domain. In the example calculated, $\alpha(t)$ gets as large as 0.3, which indicates an echo amplitude roughly an order of magnitude greater than the maximum two-pulse echo amplitude calculated for Cs in Chapter II.

If the magnetic field gradient is quadratic instead of linear, the characteristic time of Eq. (48) in the region of the plasma where H is an extremum will be

$$T = \frac{\pi\omega_c}{(1/H)(\partial^2 H/\partial x^2)\ 2\langle v^2\rangle} \cdot \frac{1}{\nu_c \tau} \tag{52}$$

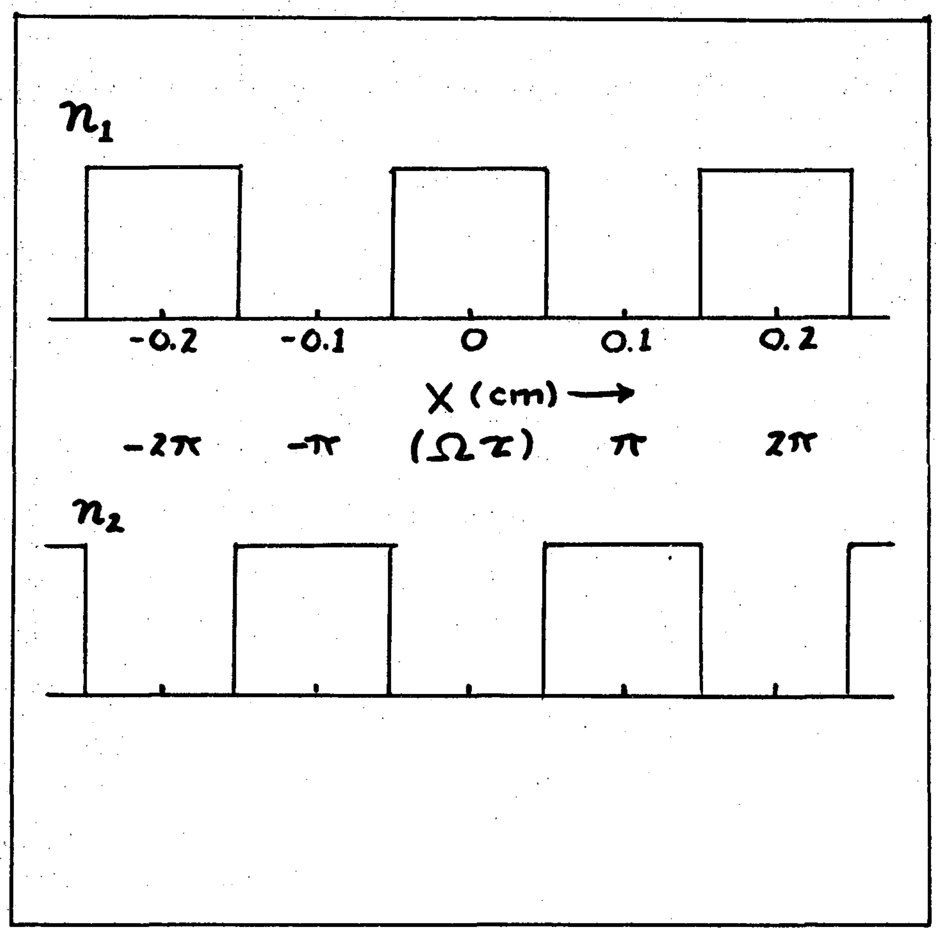

Figure 7. Hot and cold electron spatial distributions after two pulses.

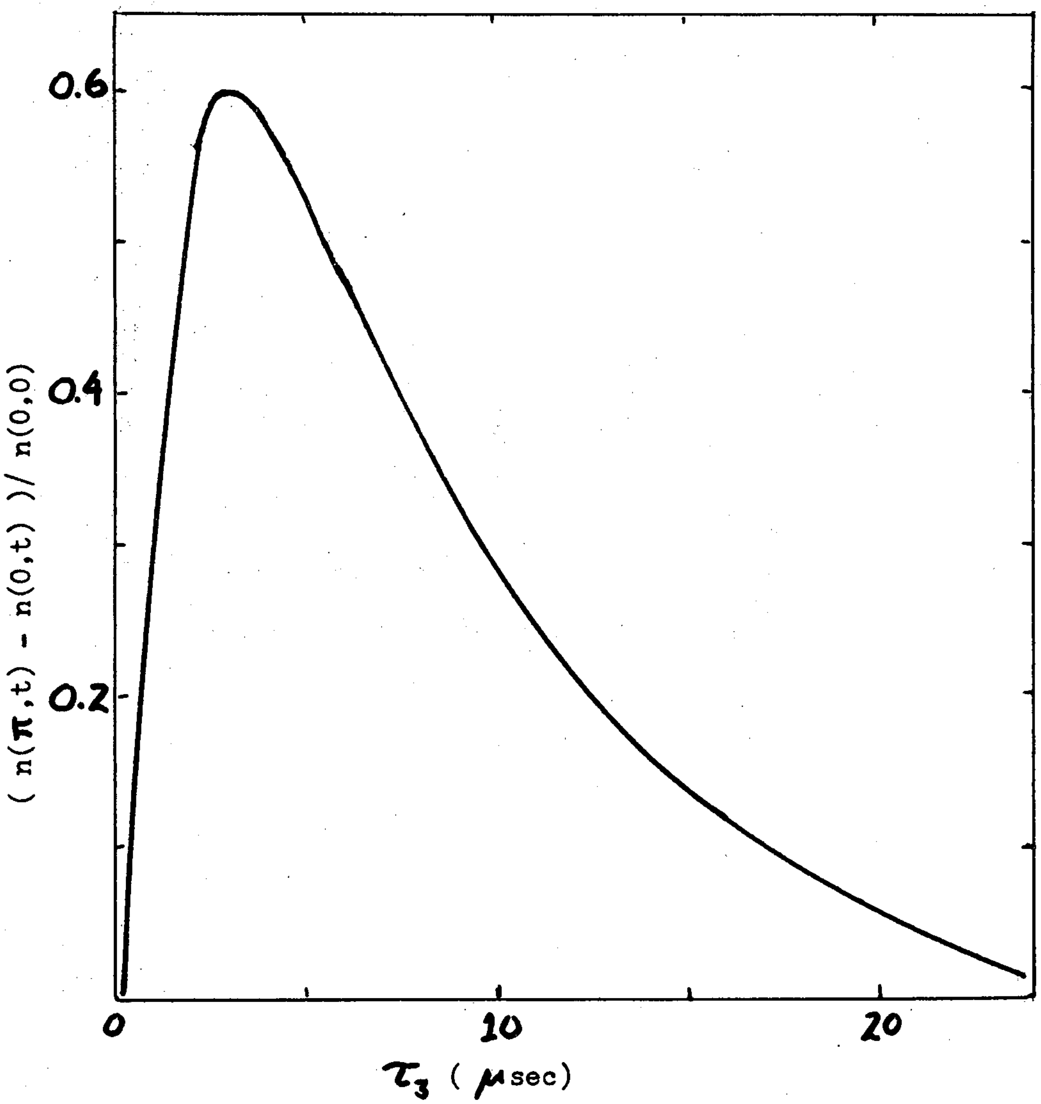

Figure 8. Calculated electron density fluctuation as a function of time after the second pulse.

where ω_c is local cyclotron frequency. In other regions of the plasma T will be shorter. Thus, for a linear gradient, one expects a fairly sharp peak in the three-pulse echo amplitude, for which T varies inversely with the neutral atom density and inversely with the square of τ. On the other hand, for a quadratic gradient, one expects a broader peak, and one for which T varies inversely with the neutral atom density and inversely with τ. For field gradients higher than quadratic, T varies inversely with some lower power of τ.

The motion of the electrons, once they start scattering is not restricted to the plane transverse to H. In Chapter II we showed that some of the transverse velocity may be scattered into the longitudinal degree of freedom. Since this is the case, and typically in these experiments there is a variation of H along the flux lines, we shall now consider the same mechanism acting on the diffusion of electrons along the flux lines. We assume that after one scattering event, the longitudinal velocity is a measure of the velocity acquired by the electron from the first two microwave pulses. Along a single flux line, there are regions where the local frequency satisfies $\Omega\tau = 2\pi n$, where n is an integer. In these regions, the electrons originally have a large transverse velocity, so after a few collision times these will be regions of hot electrons. Since the longitudinal mobility is so much greater than the transverse mobility, we shall ignore the motion of an electron away from its original flux line. Then the altering of the spectral distribution function proceeds as in the transverse diffusion case.

For diffusion along the flux lines,

$$D = \frac{v^2}{2\nu_c} , \qquad (53)$$

again from Feller's random walk treatment.[38] If this diffusion coefficient is used in the linear and quadratic field cases, we have characteristic times as before:

$$T = \left[\frac{\pi mc}{e(dH/dx)}\right]^2 \frac{\nu_c}{2v^2\tau^2} \tag{54}$$

the linear gradient, and

$$T = \left[\frac{\pi mc}{e(d^2H/dx^2)}\right] \frac{\nu_c}{2v^2\tau} \tag{55}$$

for the quadratic gradient. Both of these characteristic times show the same dependence on τ as in the transverse diffusion case, but they increase linearly with the neutral atom density. Therefore, it would be in principle possible to distinguish between transverse and longitudinal diffusion.

This longitudinal diffusion model suffers from a grave defect, however. One cannot ignore the effect of space-charge on the electronic motion along the flux lines. Any space charge fields in excess of 1 volt/cm along a flux line will profoundly modify the electronic motion. Since a spacial modulation in the electron density of less than 1% is sufficient at the electron densities used in our experiments to generate space charge fields of several volts per centimeter, the free diffusion model breaks down.

The usual treatment of space-charge limited diffusion (ambipolar diffusion)[39] requires that there be only one kind of carrier of each charge. By this is meant that all the carriers of one charge have the same mobility.

If the electron and ion densities are large enough so that the free diffusion of electrons would produce non-negligible space-charge fields, then the electrons must drag the ions along with them, so their effective diffusion coefficient is lowered. The ambipolar diffusion coefficient may be written[40]

$$D_a \approx D_i \left[\frac{T_e}{T_i} + 1 \right] \tag{56}$$

where D_1 is the ion free diffusion coefficient and T_e and T_1 are electron and ion temperatures.

However, our model has assumed two mobilities for two kinds of electrons. Since the mobility of even the cold electrons is much greater than that of the ions, these electrons will rapidly damp out any space charge. In a space-charge field of 1 V/cm, the drift velocity of the cold electrons even assuming a collision rate of 10° sec^{-1} is 10^7 cm/sec. Thus, the electrons can damp out any modulation in electron density over several centimeters along the flux lines in a time of the order of 100 nsec. Any smaller magnitude of modulation of the electron density could not account for the size of the three-pulse echoes.

Another mechanism for three-pulse echo generation has been presented by Crawford and Harp.[19] They divide the electron distribution into four parts according to whether the electron has scattered or not during $0 < t < \tau$ or $\tau < t < T'$. Crawford and Harp show that 1) those electrons which are not scattered before $t = T'$ will not in general generate a three-pulse echo unless $\tau_3 = n\tau$, where n is an integer; 2) those electrons which are scattered in both time intervals generate no three-pulse echoes at all; 3) those electrons which are scattered only during $0 < t < \tau_3$ generate echoes spaced by multiples of τ_3 after the third pulse (just a two-pulse echo for the second and third pulses); and 4) those electrons which are scattered only during $\tau < t < T'$ generate multiple echoes spaced by τ after the third pulse. Thus this last group, the coherent-scattered group, is the only possibility for generating the observed three-pulse echoes without diffusion.

In order to see the processes involved when this last group of electrons generates a three pulse echo, we show in Fig. 9 the velocity distribution of a particular isochromat before and after the third pulse. We assume several scattering times have elapsed for all isochromats, so that the velocities for each isochromat is distributed uniformly over a sphere, shown in cross section in Fig. 9a. (Of course the sphere in phase space becomes elongated along the magnetic field as time passes.) To get the average velocity of the isochromat after the third pulse, $\langle v(\Omega)\rangle$, we average over the spherical angles:

$$\langle v(\Omega)\rangle = v_o \left[\left|\cos \frac{\Omega\tau}{2}\right| + 1\right] e^{i\Omega(t-T')} \tag{57}$$

The decay terms due to scattering for $0 < t < \tau$, $t > T_3$ have been omitted, since we are assuming τ is short compared to a scattering time. Since the term in brackets is periodic in Ω, writing our usual Fourier expansion,

$$P(t > T') = \sum_n a_n G(t - (T' + n\tau)), \tag{58}$$

where a_n is the nth Fourier coefficient of $(|\cos \frac{\Omega\tau}{2}| + 1)$. Thus, we get echoes spaced by τ in the time domain.

There are two decay mechanisms for these echoes. First, any scattering during $0 < t < \tau$ and $T' < t < T' + \tau$ will degrade the amplitude of the first three-pulse echo. Secondly, diffusion in the inhomogeneous field will degrade the echo amplitude. In order to explain the effect of these decay mechanisms on the echo envelope, we shall anticipate the experimental section and define a time T_1. If the echo

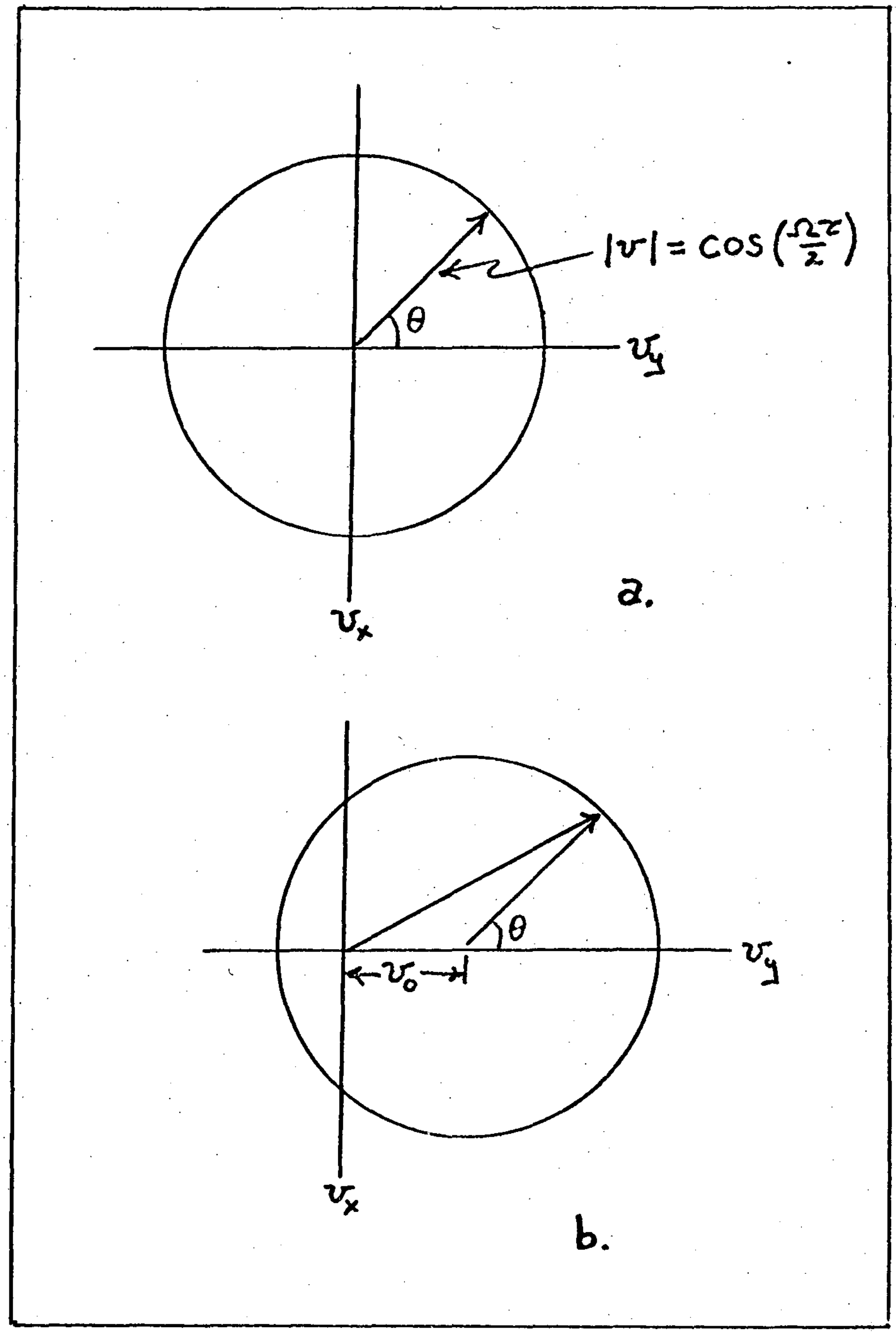

Figure 9. Electron velocity distribution before (a) and after (b) the third pulse for a particular isochromat of the coherent - scattered group.

amplitude is plotted as a function of τ_3, with the neutral atom density and τ held constant, there will be a single maximum for echoes generated by this coherent-scattered group. The τ_3 for which this maximum occurs will be denoted T_1.

We have already seen that the characteristic diffusion time, T, in the plasma is proportional to $1/\tau^2$ for a linear field gradient and $1/\tau$ for a quadratic field gradient. Also, it is proportional to n, the neutral atom density, for diffusion along a flux line, and to $1/n$ for diffusion across a flux line. This is qualitatively because diffusion across flux lines requires collisions, while diffusion along flux lines is slowed by collisions. For a given n and a quadratic field gradient, for example, we would expect T_1 to be roughly proportional to $1/\tau$. That is, as τ gets larger, the distance between regions where $\Omega\tau = 2\pi n$ decreases, and the echo is degraded more quickly by diffusion. Finally, for this model for a given τ, as n is increased, the scattering time is decreased, and the diffusion time across flux lines decreases, so T_1 can be expected to shift toward smaller τ_3. If the diffusion is primarily along flux lines, the diffusion time increases with n, and the peak described by T_1 broadens.

Three-pulse echoes showing behavior described by two of these mechanisms have been observed. These are shown with the data and discussion in Chapter IV.

"A real life plasma is a very complicated phenomenon."

Heald and Wharton [42]

IV. EXPERIMENTS AND DISCUSSION

The requirements for observing cyclotron echoes, or any echo phenomenon, are a source which generates pulses of radiation (or waves) with a pulse width less than the homogeneous relaxation time of the system, a system which can be made resonant with the input pulses and which radiates strongly enough to be detected by the necessary wide-band receiver, and a receiver with enough bandwidth so its temporal response will resolve the echoes. For the cyclotron echo experiments reported herein, the transmitter consisted of a Varian X-13 CW X-band microwave klystron followed by a Litton 10 watt grid modulated travelling wave tube amplifier (TWTA). Circuit diagrams for the blocking oscillators used to drive the grid of the TWTA were kindly provided by Dr. D. E. Kaplan. When working properly this system was capable of producing groups of three ten watt pulses, with pulse widths variable from seven to fifteen nanoseconds, at preset times. The pulses, however, could not be brought closer than 50 nanoseconds from one another without degradation of the second pulse power.

The microwave pulses were propagated from a horn antenna toward the sample, which was in an oven between the pole faces of a 12" magnet. The direction of propagation was perpendicular to the magnetic field. After passing through the sample, the transmitted pulses, and echoes were picked up by another horn antenna and passed on to the receiver.

After passing through suitable attenators, the signals were amplified by a Watkins-Johnson gated low-noise TWTA. This LNTWTA was gated off during the time the transmitted pulses were coming through to prevent saturation of the rest of the receiver chain. Following the LNTWTA was an LEL superheterodyne receiver with a 250 MHz IF and a 100 MHz bandwidth. The 250 MHz signal was amplified directly in an IFI wide band amplifier and video detected. Several stages of video simplification preceded the actual display of the signal on the Teletronix 3S76 sampling oscilloscope. Finally, since the sampling gate could be manually set, the sampling oscilloscope was used as a box-car integrator with a very short gate. The output from the sampling oscilloscope was further filtered, giving an overall integrating time of about one second, and recorded on an x-y recorder. With an overall noise figure of about ten db, this receiver had a noise limit of about -84 dbm. Echoes were measured to within 4db of this figure. Since the maximum echo powers detected in these experiments were -40 dbm, the receiver system had a dynamic range of 40 db. The overall time response was about five nanoseconds rise time and about fifteen nanoseconds fall time.

In these experiments the inhomogeneously broadened electron system was a weakly ionized cesium plasma in an inhomogeneous magnetic field. The Cs cell consisted of a cylindrical pyrex discharge bulb (9 cm long, 5 cm diameter) that was kept typically at 200°C, and a long side-arm containing a Cs puddle at a temperature that could be varied between 70° and 110°C. After pumping the cell out to 10^{-7} torr, it was baked for 12 hours at 430°C, filled with Cs by the process described by Miller,[10] and sealed off. The purity of the cell was checked, after several months of use, by examining the spectrum of the discharge. A Jarrel-Ash 1/4 meter spectrometer and a photomultiplier were used to observe the Cs lines at 4555Å and 4593Å. These lines had a signal-to-noise ratio of 10:1 and 5:1 respectively, and no other lines were observed over the photomultiplier sensitivity range of 4000-5000Å. These lines were also observed visually, and no other lines were seen over the sensitivity range of the eye. The lack of spectral lines from materials other than Cs, and the fact that the electron - Cs scattering cross-section is an order of magnitude greater than that for scattering from any other common material (except other alkali metals) was taken as good indication that electron - Cs collisions were the dominant electron relaxation mechanism. In particular this spectral evidence ruled out the possibility of nitrogen or other alkali metals significantly contaminating the system.

The Cs vapor in the discharge bulb was ionized by the electric field of a 20 MHz pulse. Metal plates at both ends of the discharge bulb formed the capacitor of a 20 MHz tank circuit. The discharge pulse typically was several tenths of a millisecond long and one kilowatt in power. The repetition rate for this discharge pulse was about 150 $sec.^{-1}$ After the discharge pulse produced the ionized gas, the electron density decayed with a time constant of about 1/5 millisecond. Therefore, the electron density could be varied at will by initiating the sequence of microwave pulses at different times in the afterglow. A schematic diagram for the whole apparatus is shown in Fig. 10.

The inhomogeneous magnetic field in these experiments was achieved by moving the discharge bulb out toward the edge of the gap between the pole faces. The measured inhomogeneity across the 5 cm cell diameter was about 25 gauss in 3000 gauss. The configuration of the inhomogeneity was roughly quadratic with maximum field toward the radial center of the gap. The inhomogeneity along the cell axis was about 20 gauss in 4 cm. Again, the configuration was roughly quadratic with the minimum field at the center of the cell, and the field rising by roughly 20 gauss at either end of the cell. This kind of an axial graident corresponds roughly to 120 regions along the axis where $\Omega\tau = 2\pi n$ for $\tau = 200$ nanoseconds, with these regions becoming more dense toward the edges. Since the plasma

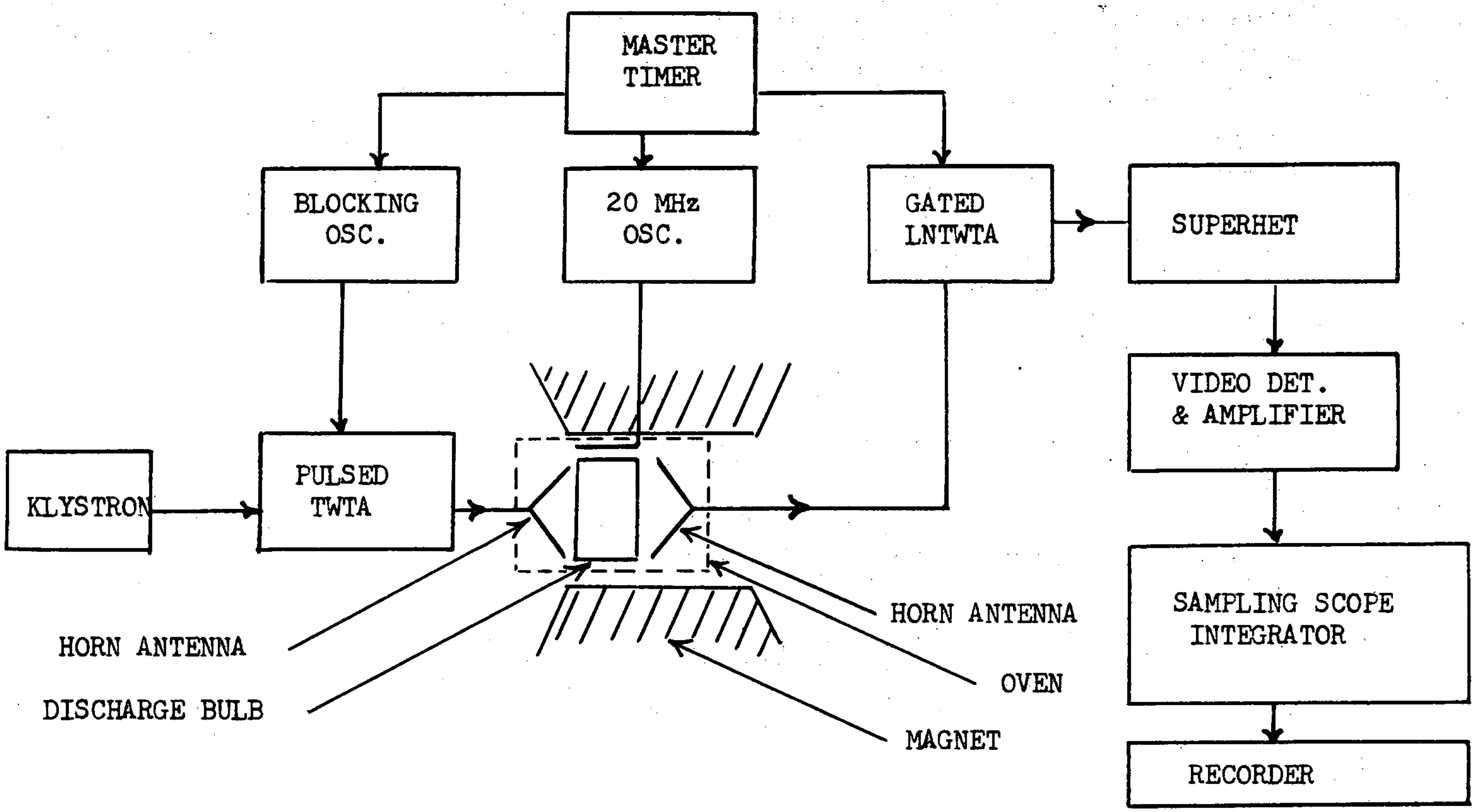

Figure 10. Block Diagram of the cyclotron echo apparatus.

probably was confined more to the middle of the cell, the average distance between hot regions was probably considerably larger than the 2/3 millimeter indicated by the above numbers.

Since a cylindrical geometry was used, and the plasma dimension was not too large, it was decided that an interferometric measurement of the electron density would not be possible. Therefore, in order to be sure that the Cs was weakly ionized, an indirect estimate of the electron density had to be made. It is well known[43] that when electromagnetic radiation propagates through a plasma in a direction transverse to a static magnetic field, and if the polarization of the radiation is such that the electric field is perpendicular to the static magnetic field, then a resonant absorption occurs at $\omega_{uh} = \sqrt{\omega_c^2 + \omega_p^2}$, where ω_c is the plasma frequency. Since ω_p is proportional to the square root of the electron density, ω_{uh} is a measure of this density. When $\omega_p \ll \omega_c$, a further reduction in electron density will not change ω_{uh}. By waiting a time from 0.3 to 0.7 msec after the discharge pulse, depending on the Cs density, it was found that the ω_{uh} was constant. For earlier times, ω_{uh} increased as the microwave pulse approached the discharge pulse. We can then place an upper limit of 10^9 cm^{-3} for the electron density at the time when ω_{uh} becomes essentially constant. Notice that this scheme does not require an absolute measurement of ω_{uh}. Then, since the Cs density was of the order of 5×10^{12} cm^{-3} in these experiments, we may say that the gas was less than 0.1% ionized.

The fact that the gas was weakly ionized was necessary to assure us that we were not measuring electron-ion screened Coulomb collisions instead of electron-neutral collisions. The Coulomb collisions have already been observed in a strongly ionized Cs plasma.[21] For electron and ion densities of 10^9 cm^{-3}, and electron velocities of about 1 (e.v.)$^{1/2}$

the screened Coulomb momentum change cross section[44] is about 10^{-14} (cm^2). Since this is about 1/3 the electron-neutral cross section, we see that an ionization of greater than 50% is necessary before this collision mechanism becomes important.

The behavior of multiple two-pulse echo powers as a function of τ is shown in Fig. 11 along with theoretical calculations based on Eq. (21). Figure 12 makes the same comparison for several different Cs densities, and Fig. 13 makes the same comparison for several input pulse areas (i.e. pulse power). For the calculated curves the Cs density in the discharge bulb was taken as $n = n_{SA} (T_{SA}/T_B)^{1/2}$, where n_{SA} is the vapor density corresponding to the temperature of the Cs puddle in the side-arm, T_{SA}, and T_B is the temperature of the discharge bulb. It was assumed that the temperature of the gas in the discharge was not significantly different from the temperature of the walls, since the Cs neutral atom mean free path was a large fraction of the bulb diameter. The Cs vapor pressure was taken from Smithells.[45] Typically side-arm temperatures ran from 79°C to 105°C, corresponding (after the above correction) to 3.6×10^{12} to 2×10^{13} cm^{-3} Cs density. It was found after comparing the data with the theory that the agreement was better if the calculated density was reduced by 30%. In view of the well known[10] difficulty of making accurate measurements of vapor pressure vs temperature, this correction does not seem unreasonable. It was probably a systematic error in reading the temperature of the Cs puddle.

If the self-diffusion of electrons along the flux lines into regions of different magnetic field were an important relaxation mechanism, the characteristic relaxation time it would introduce would be proportional to the Cs density from arguments similar to those used in Chapter III.

However, if the electronic mean free path in the direction of the flux lines is long compared with the characteristic distance in which the cyclotron resonance frequency changes by $2\pi/\tau$, the diffusion model breaks down. In this case, the degradation in echo power due to self-diffusion should be independent of the Cs neutral density. Herrmann, et al.,[13] have shown that including the collisionless electron drift along flux-lines results in a decay in the echo envelope which depends upon the exact form of the magnetic field inhomogeneity. In particular, for a quadratic variation, they find an attenuation factor proportional to $\tau^{-2}\,\mathrm{erf}(c\tau^2)$, where c is a constant. As is seen from the agreement in Fig. 12 between the data and the theory without diffusion or drift, these effects do not appear to be important.

Also, all the theoretical curves are multiplied by a single overall scale factor to bring them into agreement with the observed echo power. Since the echo power is proportional to the square of the total number of electrons, and this number was not known with any certainty, this scaling was necessary. As we shall show, however, the order of magnitude is correct.

Classically, the electric dipole field from a circulating electron is given by

$$E = \frac{p}{r^3} \tag{59}$$

where $p = eR_c$, the electron dipole moment. The total dipole field at the edge of the plasma is

$$E_{\mathrm{total}} = N \frac{e\,R_c}{\langle r^3 \rangle}\; f, \tag{60}$$

where f is the calculated factor $\tilde{P}/v_0$, N is the total number of electrons,

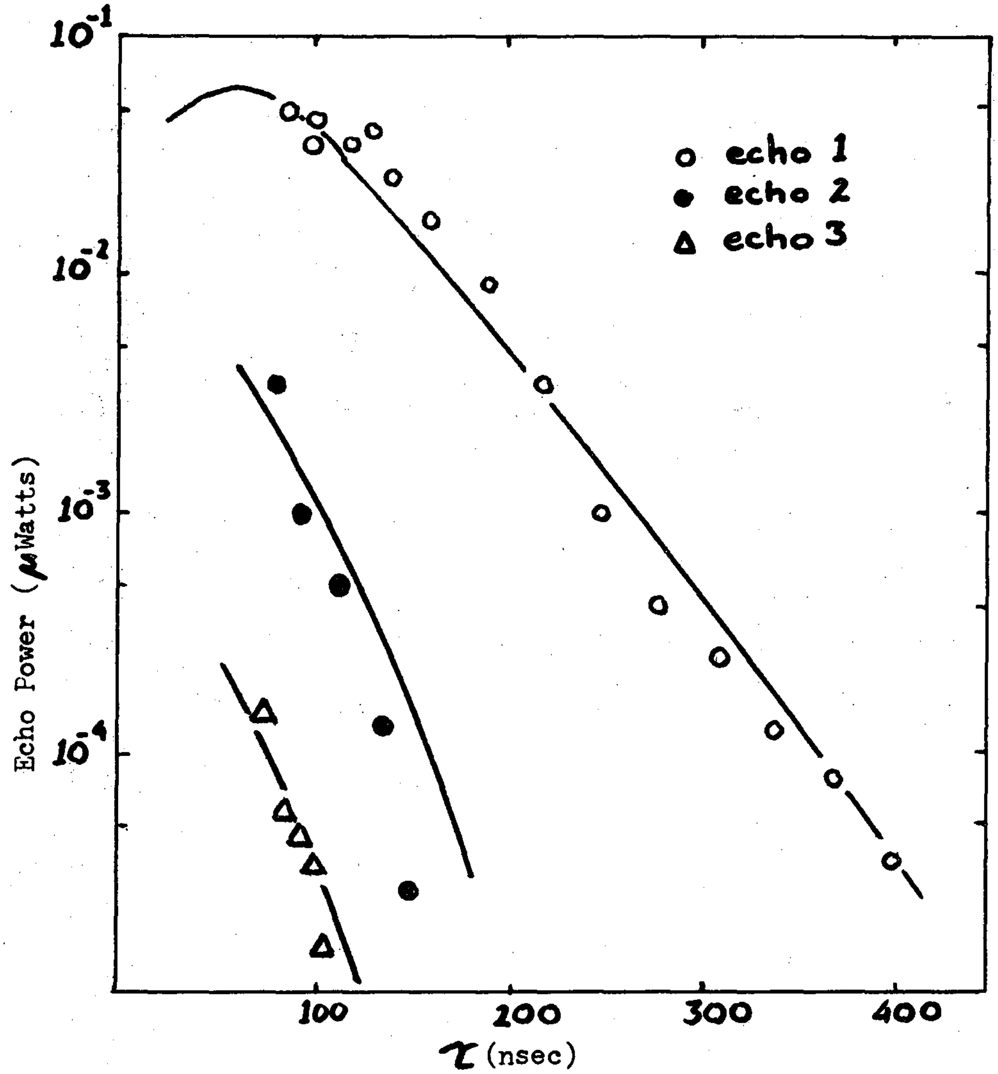

Figure 11. Theoretical (solid curves) and experimental two - pulse echo power for the first three echoes. The data was taken at a Cs pressure, corrected as described in the text, of 1.2×10^{-4} Torr.

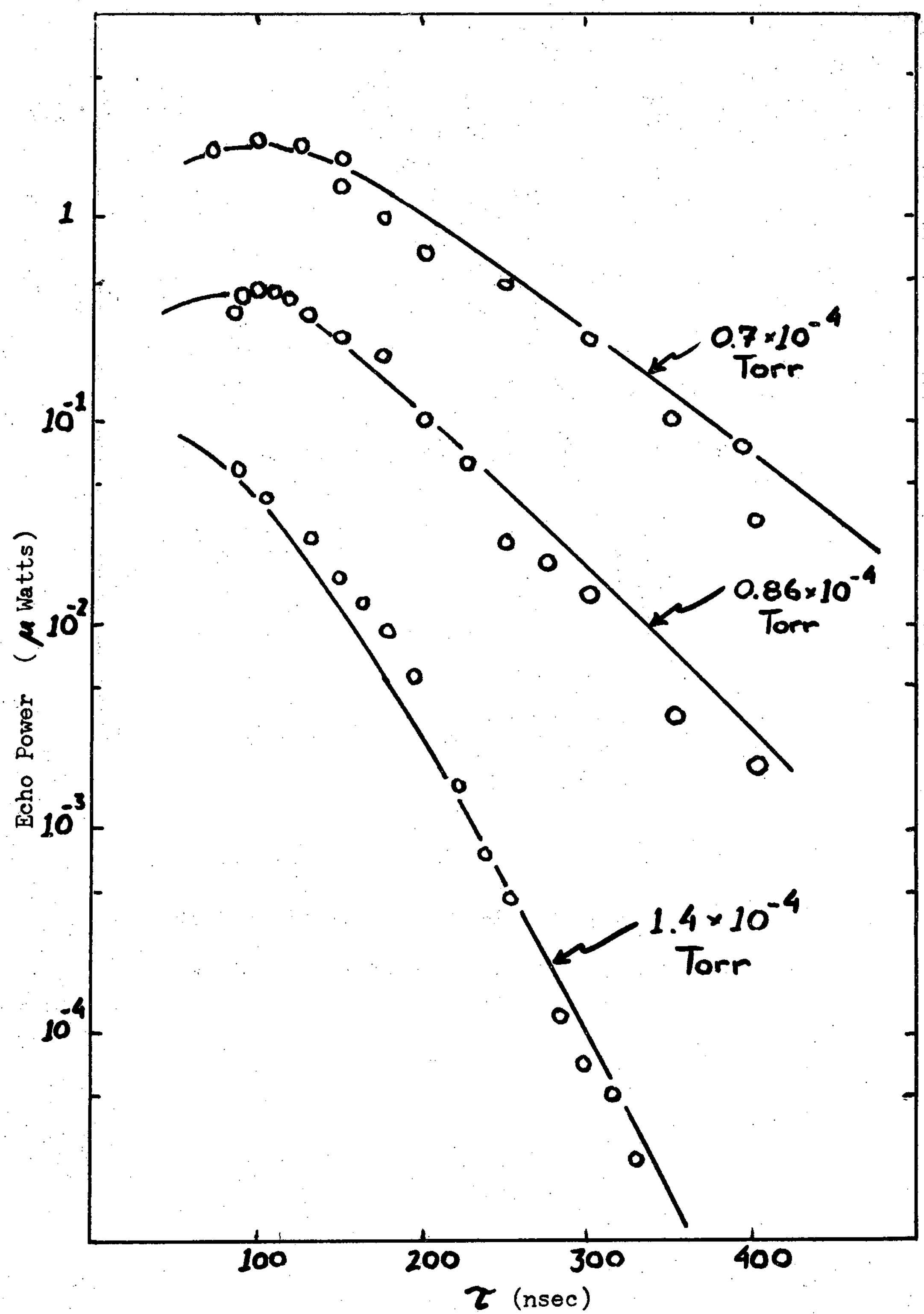

Figure 12. Theoretical (solid curves) and experimental two-pulse echo powers for several Cs pressures. Data for 0.86 and 0.7 x 10^{-4} Torr have been multiplied by 10 and 100 respectively.

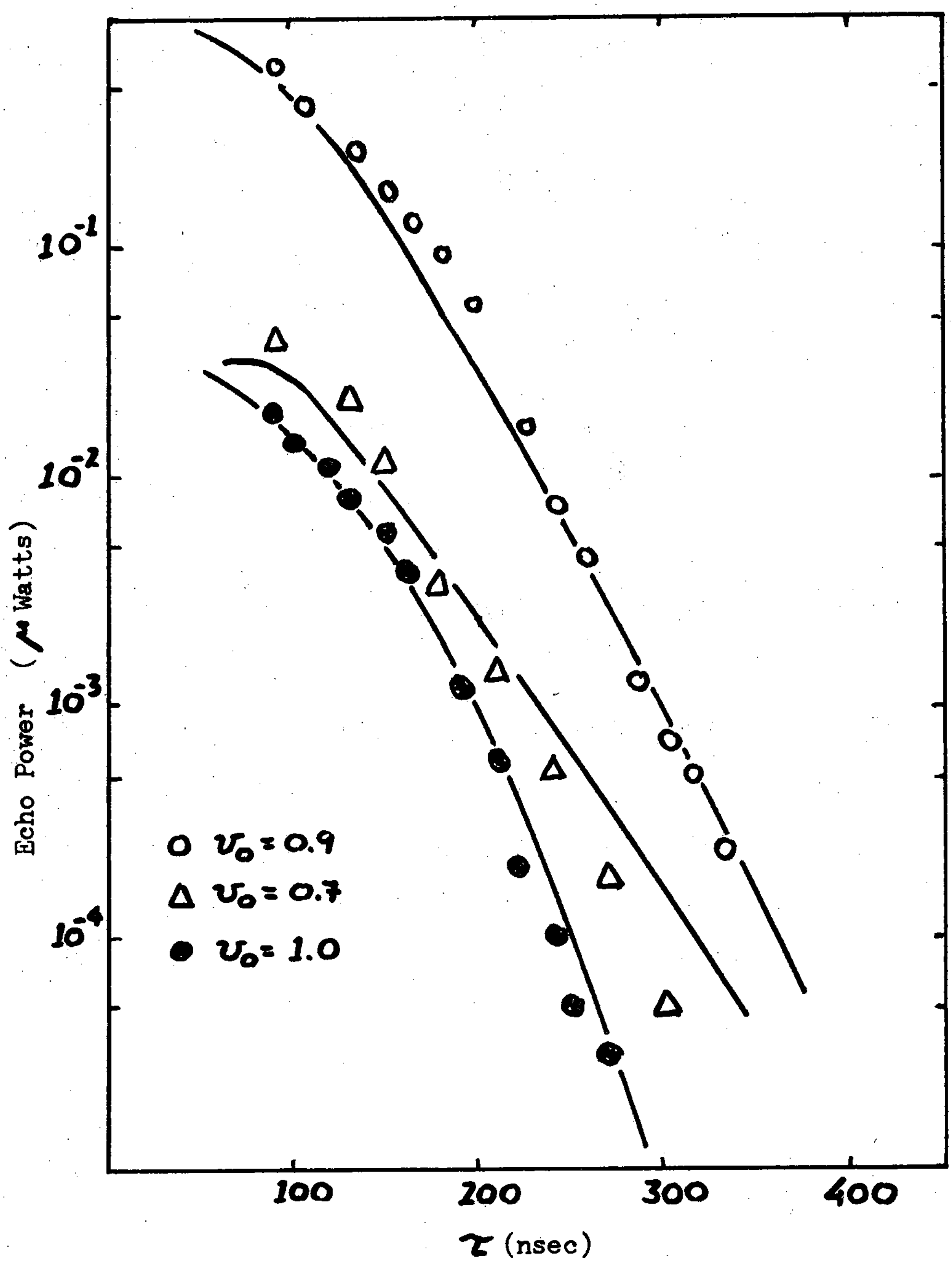

Figure 13. Theoretical (solid curves) and experimental two-pulse echo powers for several input pulse powers. The data for $v_o = 0.9$ has been multiplied by 10 for clarity in the graph. The corrected Cs pressure was 1.4×10^{-4} Torr.

and we have integrated over the plasma volume. Since $N/\langle r^3\rangle \approx n_e$, the electron density, we can write the energy flux from the plasma as

$$S = \frac{1}{4\pi} (n_e e R_c f)^2 c, \qquad (61)$$

where c is the speed of light. Putting in the experimental numbers of $n_e = 10^9$ cm^{-3}, $v_0 = 1$ (e.v.)$^{1/2}$, and the calculated f of 10^{-2}, $S \approx 4\times10^{-9}$ watt/cm^2. Then, assuming the echo power comes out as a plane wave, since the receiver horn presents a 25 cm^2 cross section, the received power should be roughly 10^{-7} watt, in good agreement with the measured maximum echo power. This figure is two orders of magnitude below the maximum echo power for an Argon plasma used to tune up the apparatus, also in good agreement with calculation.[46]

Finally, the relation between v_0 and the input pulse power was determined by comparing the pulse power for maximum echo with the calculated v_0 for maximum power. This parameter can also be roughly calculated, but geometrical uncertainties make the calculation uncertain by 50%. From Eq. (5), $v_0 = \frac{1}{2} \frac{e}{m} E t_p$, where E is the microwave electric field and t_p is the pulse width. In the waveguide, the maximum electric field can be written as E(e.s.u.) $\approx$ 0.1 (power (watts))$^{1/2}$, so for 1 watt E(e.s.u.) $\approx$ 0.1. The transmitter horn had dimensions between the 10 and 15 db standard gain horns, so the 3 db angular opening was roughly 40°. From the geometry of the horn and the plasma, then, the average maximum electric field in the plasma was 2.5 10^{-2} e.s.u., and for a 10 nanosecond pulse, $v_0 \approx 6\times10^{-7}$ cm/sec, or 1(e.v.)$^{1/2}$. This is seen to be not far from our experimental choice of $v_0 = 0.5$ (e.v.)$^{1/2}$ for 1 watt incident pulse power (-10 db from maximum power).

Three pulse echo behavior is shown in the next few figures. Figure

14 shows the three-pulse echo amplitude as τ_3 is varied and defines the three significant peaks. P_1 we identify with the coherent-scattered group mechanism discussed in Chapter II, in part because this is the only mechanism that does not involve diffusion and the time for the maximum of P_1, called T_1, is only a few collision times, too short for any of the diffusion mechanisms discussed. Also, P_1 is identified with the coherent scattered group mechanism because of its behavior as τ and Cs density are varied, as shown in Fig. 15. Thus, T_1 is proportional to the $1/\tau$ as we might expect for a quadratic field variation, and it decreases as n is increased, just as we predicted for the coherent-scattered group mechanism in Chapter III.

The variation of T_2, the τ_3 for the maximum P_2, as τ is varied is shown in Fig. 16, and as n is varied is shown in Fig. 17. It is seen in Fig. 17 that the behavior of T_2 as the Cs density is varied is that predicted for the longitudinal diffusion model. The difference between transverse and longitudinal diffusion can be seen qualitatively in that the transverse diffusion requires collisions, while the free longitudinal diffusion is slowed by collisions. Therefore the longitudinal diffusion time increases with density while the transverse diffusion time behaves in an opposite manner. The slope of the line in Fig. 17 also corresponds well to the characteristic ambipolar diffusion time using D_a from Eq. (53).

However, in view of the objection to this model expressed in Chapter III, we must regard this agreement as fortuitous. Another mechanism (considerably uglier) can be proposed to explain the variation of T_2 with Cs density. First, one must ask what causes maxima in the three-pulse echo envelope. One cause is the peaking of the electron density in the middle of the plasma cell. Then, at the time characteristic for diffusion of electrons between hot and cold slabs at the center of the plasma, there will be a maximum in the three-pulse echo envelope. In other words, if the magnetic field and electron density were known over the whole plasma, then the three-pulse echo envelope could be calculated by finding the distance between hot slabs (a) for each region of the plasma, calculating a curve analogous to Fig. 8, multiplying by a factor proportional to the local electron density, and integrating over the whole plasma volume. Then those regions where the electron density is large will be weighted more heavily, resulting in a maximum in the three-pulse echo envelope.

Another cause for the peaking in the three-pulse echo envelope is that there may be regions in the plasma where the field gradient is stationary. That is, if there are large regions in the plasma where the distance between hot slabs is constant, the three-pulse echo envelope will peak at the time characteristic of such regions.

Undoubtedly, as the Cs neutral density is changed, the spacial electron distribution in the plasma is changed. As an example, suppose the transverse inhomogeneity is quadratic with a minimum at the edge of the plasma bottle. At low Cs densities one might expect breakdown to occur only near the axial center of the bottle since electrons near the walls are relaxed more readily and cannot produce a discharge. As the Cs density is increased, the electron distribution after the discharge is more evenly spread over the bottle, resulting in a larger density in regions of high and low a (distance between hot slabs). The three-pulse echo envelope will then develop peaks at earlier and later times. Then as the Cs density is increased, the characteristic time for the later peak increases. Many variations on this mechanism can be invented by using different magnetic field distributions. Therefore, unless great care is taken in producing a simple magnetic field distribution, the variation of the three-pulse echo peaks with neutral density will be subject to question.

Finally P_3 was a very broad peak with weak structure in it. As τ and n were varied the various sub-peaks of P_3 varied in relative amplitude making a positive identification more difficult. Figure 18 shows P_3 for two densities with an identification of structures showing roughly the predicted variation as $1/n$. More complete data on the variation of the structure of P_3 as τ is varied are shown in Fig. 19. Again the variation is what we expect for the transverse diffusion mechanism in a quadratic field inhomogeneity. The structure, of course, would not be there if the inhomogeneity were uniform across the plasma.

Finally, in Fig. 20 we show superimposed the first three-pulse echo and a two-pulse echo from pulses two and three. The sampling scope gate was set τ (390 nsec) after the third pulse, while τ_3 was swept automatically. The resulting trace shows P_1 and the beginning of P_2. When $\tau_3 \approx 390$ nsec, a two-pulse echo is seen superimposed on P_1.

In conclusion, cyclotron echoes in a weakly ionized Cs plasma have been measured and compared with various models, with satisfactory agreement. In particular, the velocity dependent collision frequency is adequate to explain the features of the two pulse echoes. The data of Brode[29] were shown to be adequate to describe the two-pulse echoes. The combination of coherent-scattered group and transverse diffusion mechanisms were shown to describe the gross behavior of the three-pulse echoes. A description of the detailed behavior of the three-pulse echoes would

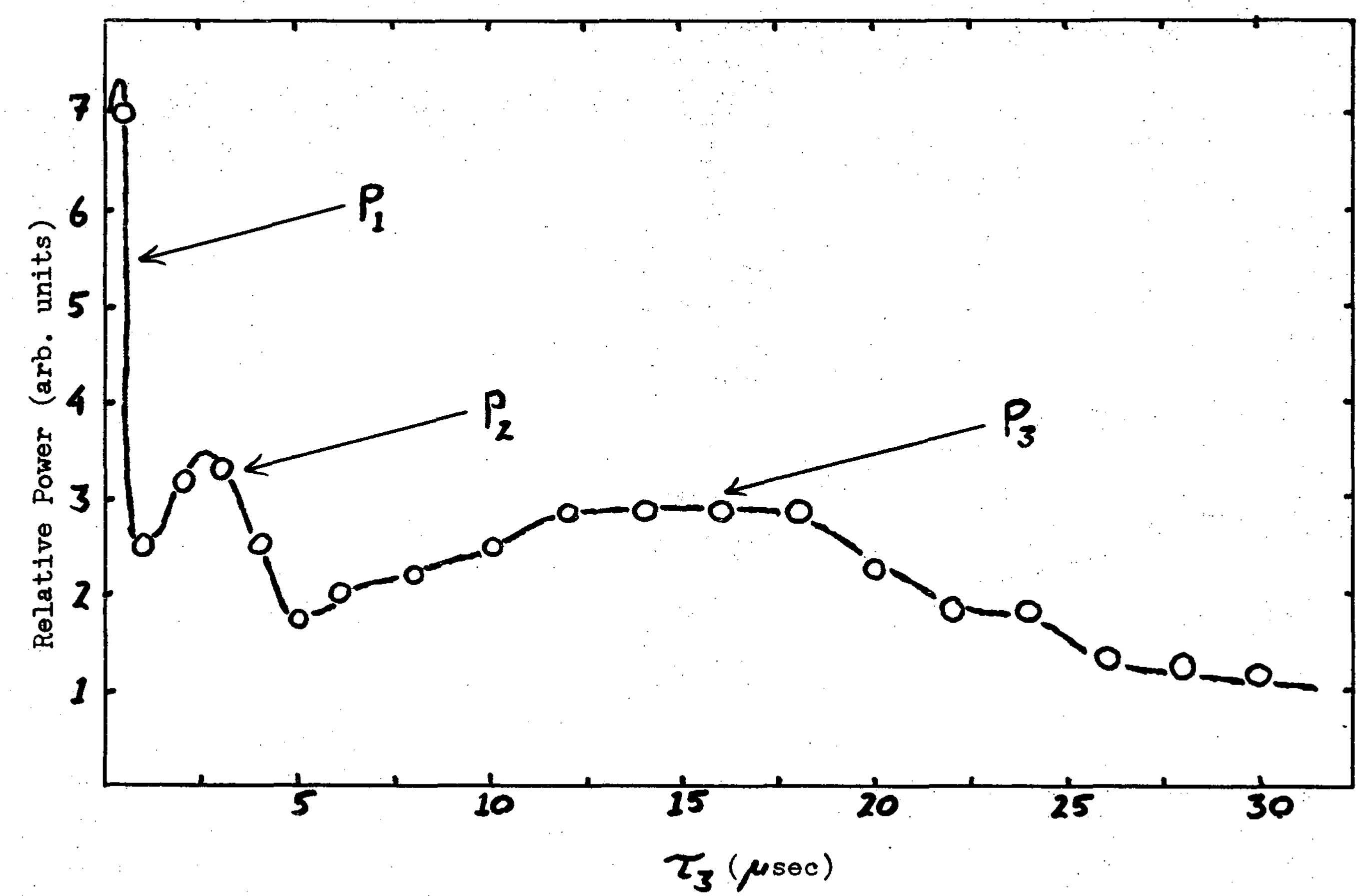

Figure 14. Structure in the first three-pulse echo envelope as a function of τ_3.
(τ = 200 nsec, Cs density = 4×10^{-4} Torr)

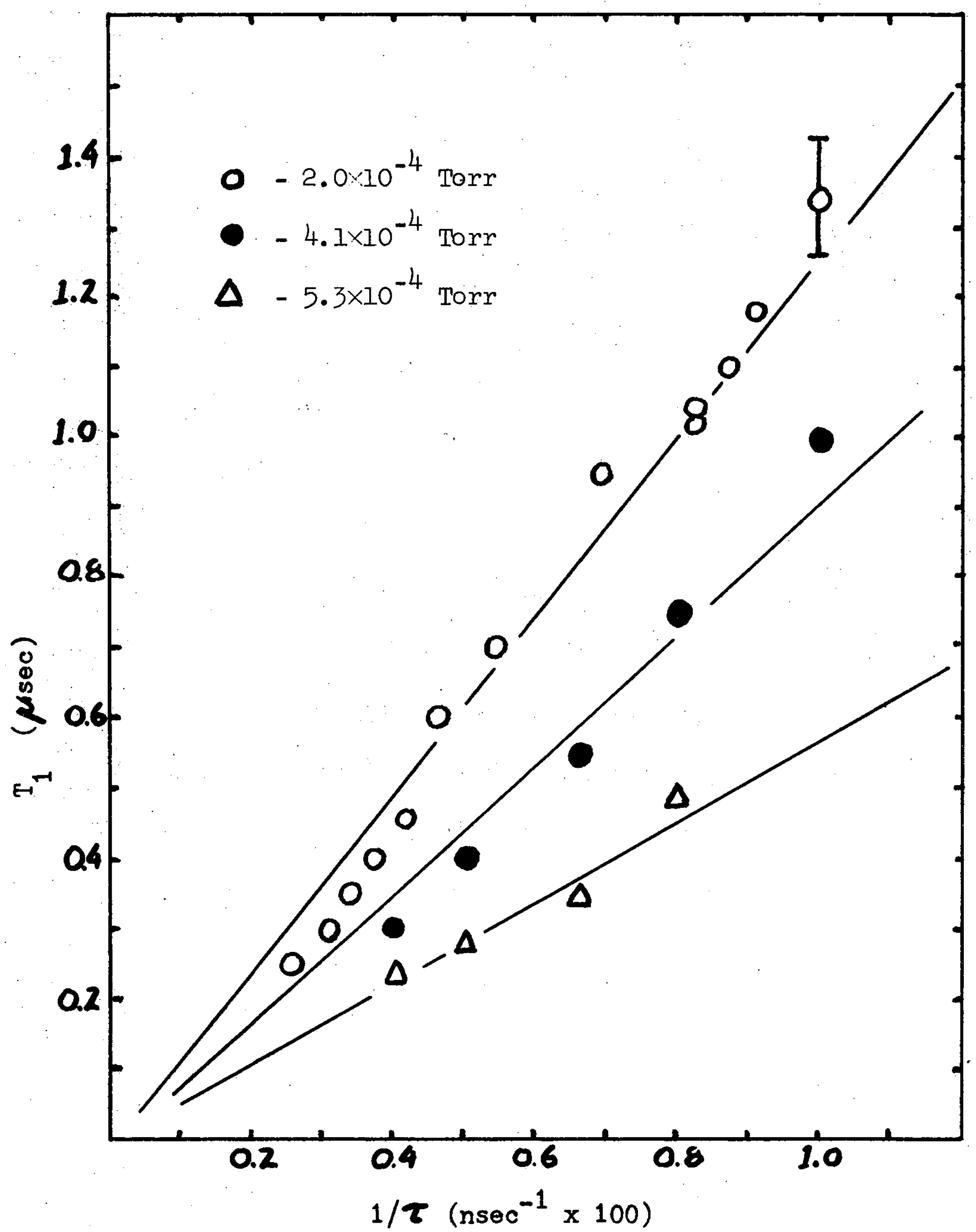

Figure 15. Variation of the maximum of P_1 as a function of the reciprocal of the two-pulse spacing for several Cs pressures. The numbers in the upper left indicate the pressures.

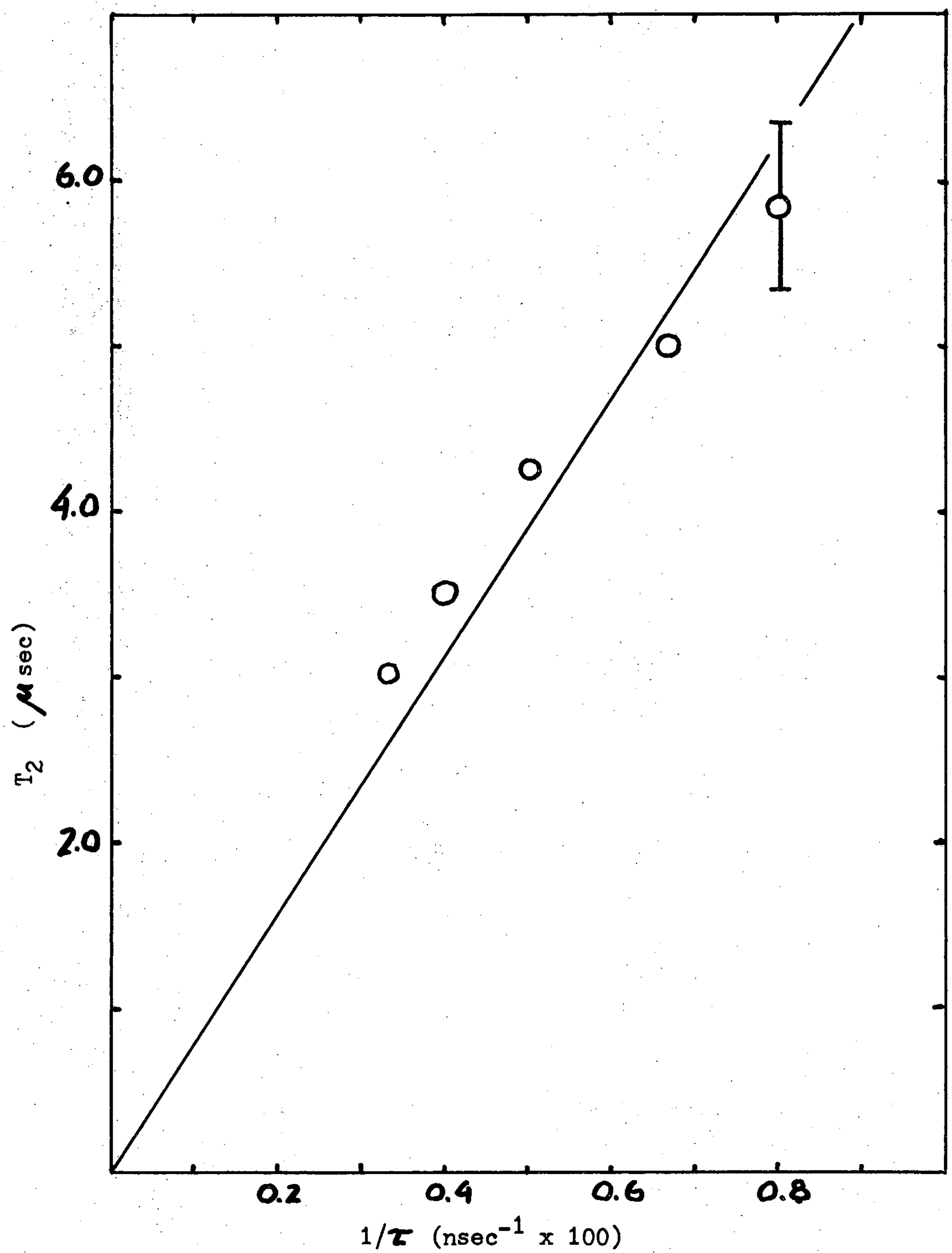

Figure 16. Variation of the time of the maximum of P_2 as a function of the reciprocal of the two-pulse spacing. The Cs pressure was 3.6×10^{-4} Torr.

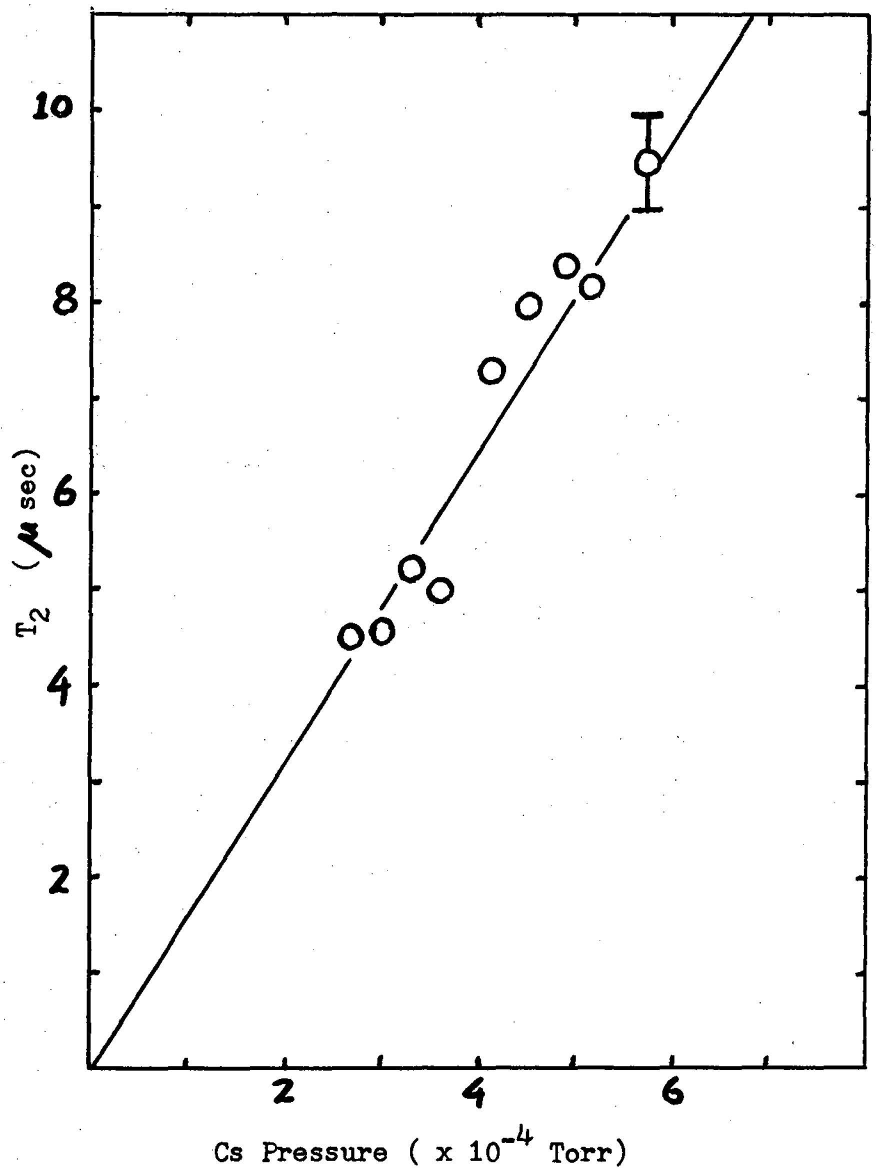

Figure 17. Variation of the time for the maximum of P_2 as a function of the Cs neutral atom density. The two-pulse spacing was 200 nsec.A typical error flag is shown indicating the estimated uncertainty in measuring T_2 and the Cs pressure.

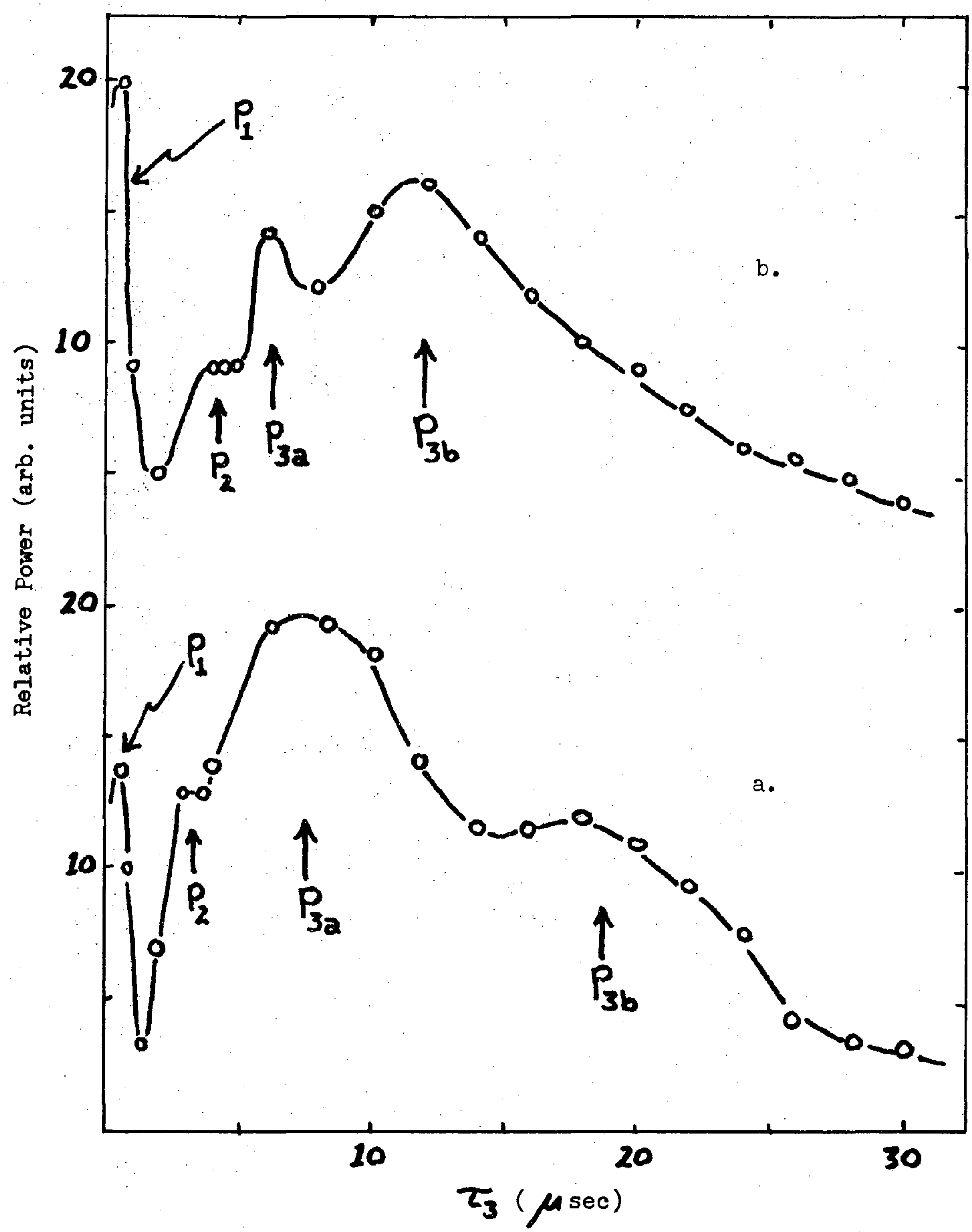

Figure 18. The first three-pulse echo envelope vs for two Cs pressures: a. 1.8 x 10^{-4} Torr, b. 2.4 x 10^{-4} Torr. The structure on P_3 is seen to be two bumps, P_{3a} and P_{3b}. Note the opposing motion of P_2 and P_3 as the Cs density is varied.

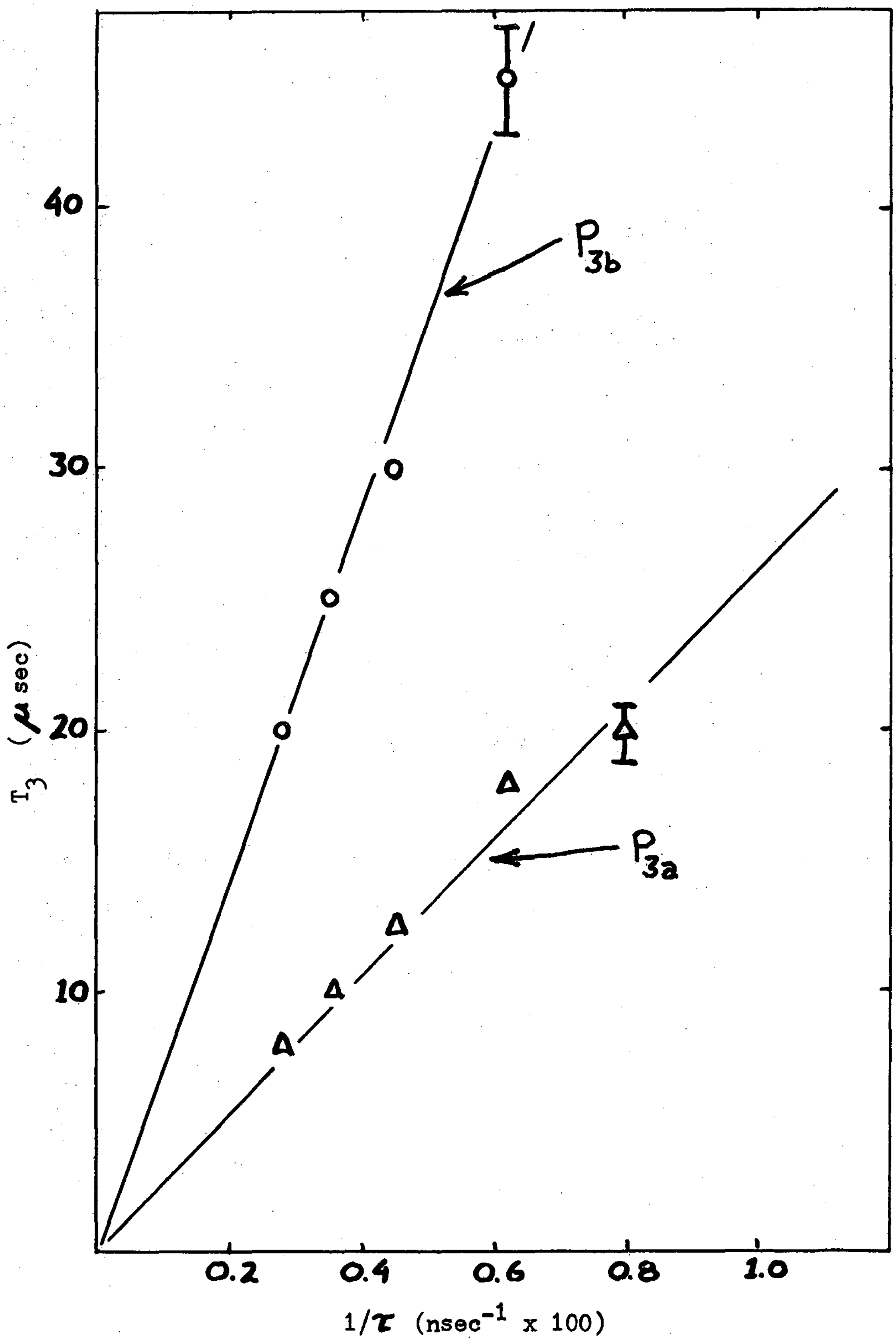

Figure 19. Variation of the times for maximum P_{3a} and P_{3b} vs the reciprocal of the two-pulse spacing.

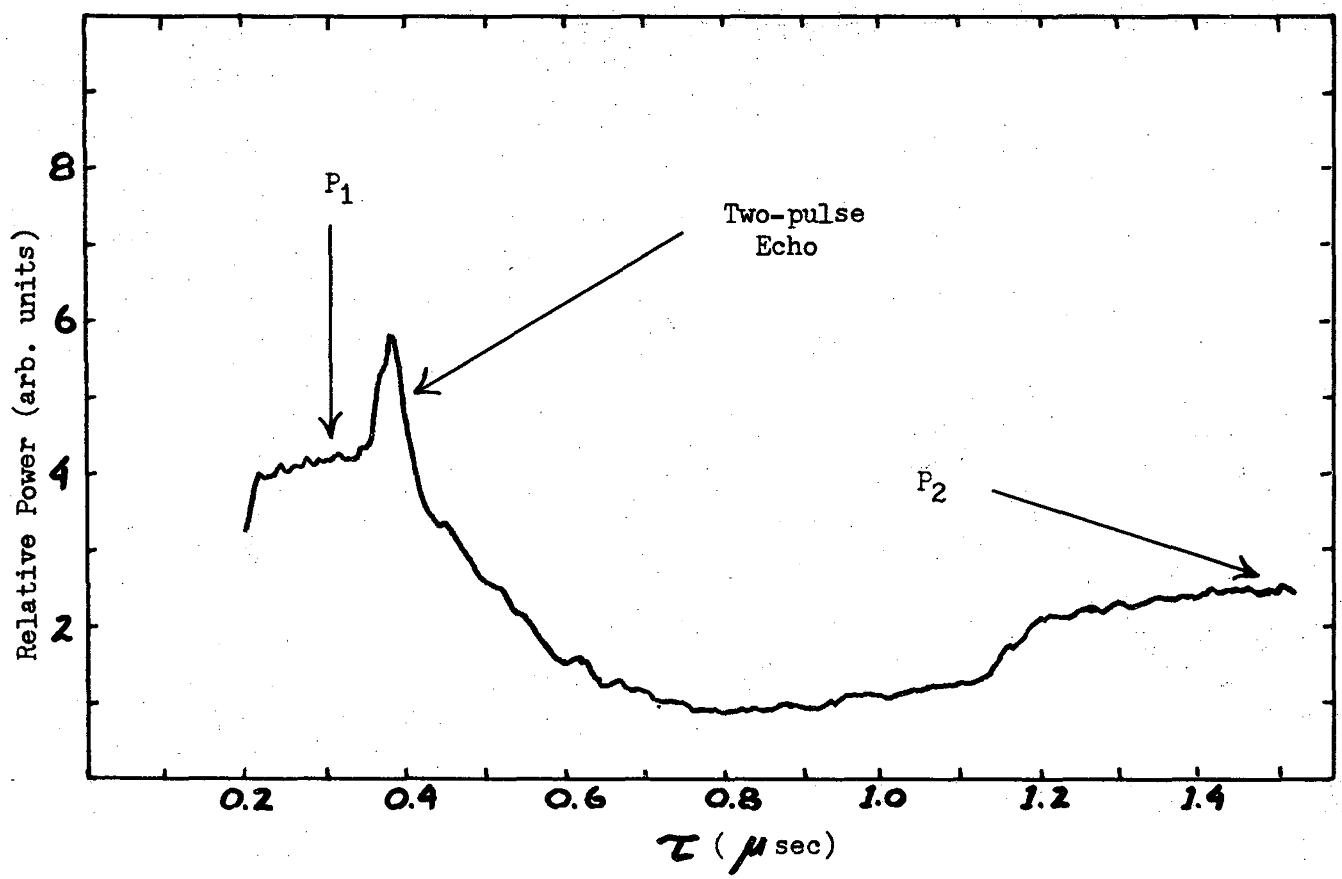

Figure 20. First three-pulse echo envelope as a function of τ_3, showing superimposed a two-pulse echo from the second and third pulses.

require an accurate knowledge of the magnetic field and electron density distributions over the plasma region. Since these quantities were not known with much accuracy in these experiments, such a detailed description was impossible. However, as a suggestion for future experiments, we would recommend examining the behavior of the echo envelope as the neutral density is increased in a plasma system with a simple (e.g. linear gradient) and accurately known magnetic field distribution.

ACKNOWLEDGEMENTS

The author wishes to thank Professor Erwin L. Hahn for his continuing advice, encouragement, and sympathetic ear, as well as financial support, during these experiments. I also wish to gratefully acknowledge the advice of Dr. Dan E. Kaplan concerning the setting up of a cyclotron echo apparatus. Long conversations with Dr. Stephan A. Miller, Dr. Sam L. McCall, and Dr. L. W. Riley have been of great help in my development as an experimental physicist. Partial financial support for this work came from the National Science Foundation and the United States Atomic Energy Commission.

Finally, I would like especially to thank Marja and Marieken for making sure physics never got the upper hand.

APPENDIX A

Two factors contribute to the degradation of the coherently radiated electric field from a scattered electron. First, since the polarization is proportional to the part of the velocity which is transverse to the magnetic field, any elastic scattering of the electron into the helical orbit reduces the transverse velocity and hence reduces polarization and radiated electric field proportionately. Secondly, as is shown in Fig. 3, a scattering angle, $\delta\psi$, in the transverse part of the velocity results in an equal phase shift and a reduction of the coherently radiated electric field by a factor of $\cos(\delta\psi)$. Figure A1 shows the geometry necessary to calculate the effect of scattering to a velocity with non-zero longitudinal component. In this figure we have that the magnitude of the velocity is unchanged by elastic scattering. Thus, $|\vec{v}'|$, the velocity after scattering is equal to $|\vec{v}|$. The component of $\vec{v}'$ in the plane perpendicular to H is the transverse velocity, v_t, and the component of v' along H is the longitudinal velocity, v_ℓ. Since $v_t^2 + v_\ell^2 = (v')^2 = v^2$, and $v_\ell = v \sin\theta \cos\chi$, where θ is the scattering angle, and χ is the azimuthal scattering angle relative to the direction of H, we have

$$v_t = v(1-\sin^2\theta \cos^2\chi)^{1/2} \tag{A-1}$$

The phase shift, $\delta\psi$, in the transverse part of the velocity is then given by

$$\cos(\delta\psi) = \frac{v\cos\theta}{v_t} \tag{A-2}$$

The component of the radiated electric field in the direction of electric field radiated by the unscattered electrons is given by

$$E \propto v_t \cos(\delta\psi) \tag{A-3}$$

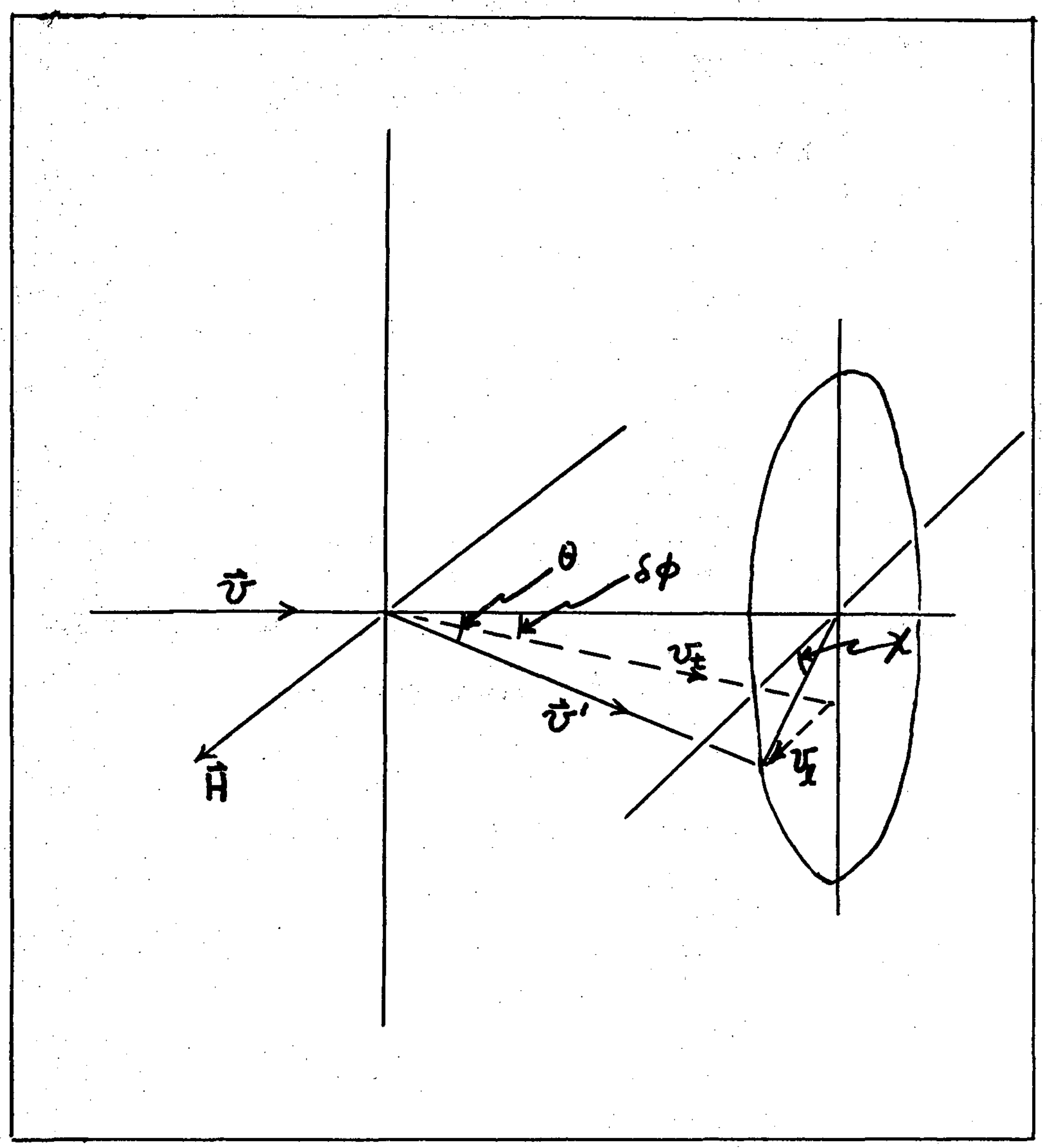

Figure A1. Geometry for a general elastic collision with scattering angle θ.

Then Eqs. (A-1)-(A-3) show that the effect of the scattering is to reduce the electric field by a factor of cos θ, just as in the case where the motion was restricted to a plane.

An implicit assumption in this derivation has been that the magnitude of the magnetic field is constant along a flux line. If this is not the case, the velocity component, v_{ℓ}, will rapidly take the electron into a region of different field, thereby further dephasing the orbit.

APPENDIX B

Analytical Results for Two-Pulse Echo Amplitude

From Eq. (21) we may write the expression for the amplitude of the first two-pulse echo:

$$a_1(t,\tau) = \frac{\tau}{2\pi} \int_{-\pi/\tau}^{\pi/\tau} \left[e^{2i\Omega\tau} + e^{i\Omega\tau} \right] e^{-\nu_c(\Omega)(t-\tau)} d\Omega \qquad \text{(B-1)}$$

Since $\nu_c(\Omega)$ is an even function of Ω, this expression can be simplified to

$$a_1(t,\tau) = \frac{1}{\pi} \int_0^{\pi} [\cos 2\theta + \cos\theta]\, e^{-\nu_c(\theta)(t-\tau)}\, d\theta \qquad \text{(B-2)}$$

where $\theta = \Omega\tau$. We shall investigate this expression and its derivative for various forms of $\nu_c(\theta)$ and then relieve the restriction that the two pulses be of the same area.

1. If ν_c is independent of θ, $a_1(t,\tau) = 0$ as was shown in Section IIC. However, one should note that this condition requires $\sigma \propto 1/v$, since $\nu_c = N\sigma v$, where v is the electronic velocity. This is indeed a severe restriction on the cross-section, and thus, one would not expect it to apply to any real collision processes.

2. In order to see the behavior of a_1 as $\tau \to 0$, we write $\nu_c(t-\tau) \ll 1$, and

$$a_1(t,\tau) \approx \frac{\tau - t}{\pi} \int_0^{\pi} (\cos 2\theta + \cos\theta)\, \nu_c\,(\theta)\, d\theta = \frac{\tau \mp t}{\pi}\, I\,, \qquad \text{(B-3)}$$

where the integral I is independent of t and τ. Two cases will be discussed in this section. One case will be for $\nu_c(v)$ a monotonic increasing function (MI) of velocity. This is the case for most electron-atom collisions up to electron energies of about one volt. The other case will be for $\nu_c(v)$ a monotonic decreasing function (MD) of velocity, which is the case for the screened coulomb electron-ion collisions. First, we show that for $\nu_c(v)$ MI, $I > 0$, and for $\nu_c(v)$ MD, $I < 0$. The function $g(\theta) = \cos 2\theta + \cos \theta$, which is plotted in Fig. B-1 is positive for $0 < \theta < \theta_c$, and negative for $\theta_c < \theta < \pi$. Since the integral of $g(\theta)$ from 0 to π is identically zero,

$$\int_0^{\theta_c} g(\theta)\, d\theta = - \int_{\theta_c}^{\pi} g(\theta)\, d\theta. \tag{B-4}$$

If $\nu_c(v)$ is MI, then $\nu_c(\theta)$ is MD. Therefore,

$$\begin{aligned}\int_0^{\theta_c} g(\theta)\, \nu_c(\theta)\, d\theta &\geq \nu_c(\theta_c) \int_0^{\theta_c} g(\theta)\, d\theta \\ &\geq - \nu_c(\theta_c) \int_{\theta_c}^{\pi} g(\theta)\, d\theta \\ &\geq - \int_{-\theta_c}^{\pi} g(\theta)\, \nu_c(\theta)\, d\theta,\end{aligned} \tag{B-5}$$

and $I \geq 0$. The result for $\nu_c(v)$ MD is proved the same way.

Since $G(t-2\tau)$ is assumed to be sharply peaked at $t = 2\tau$, the measured echo amplitude will be

$$a_1(t = 2\tau, \tau) = \frac{-\tau}{\pi} I\ . \tag{B-6}$$

Thus, for $\nu_c(v)$ MI, $I > 0$, and $a_1 < 0$ so that the absolute value of the amplitude increases linearly with τ. For $\nu_c(v)$ MD, $I < 0$, and $a_1 > 0$. In this case also the amplitude increases linearly with τ. (In fact,

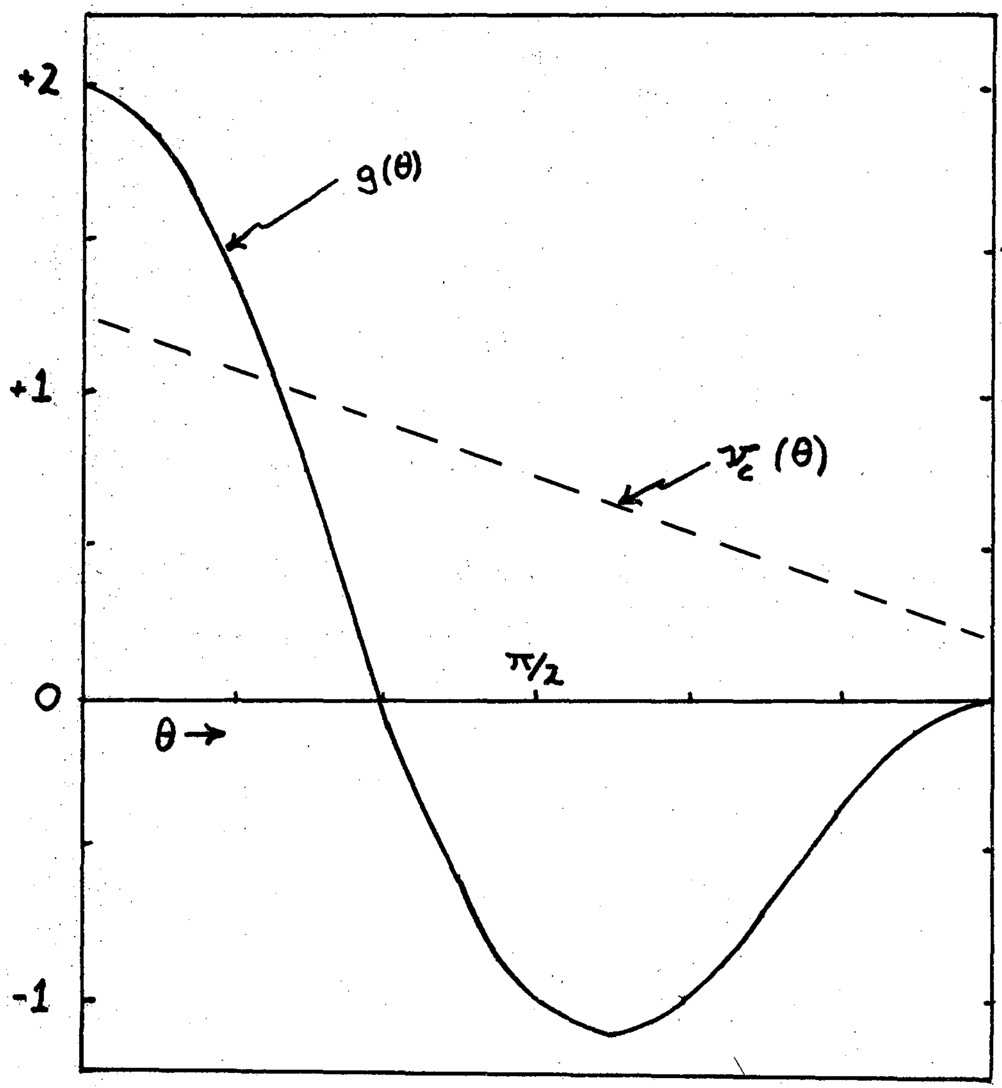

Figure B1. The function $g(\theta) = (\cos\theta + \cos 2\theta)$, and a representative collision frequency for $\nu_c(v)$ MI.

from Eq. (B-3), one can see that $a_1 \propto \tau$ for $\nu_c\tau \ll 1$, independent of the form of the collision frequency.) From this result it is clear that unless one measures the phase of the first echo relative to the phase of the input pulses, there is no way to distinguish a MI collision frequency from a MD one.

3. Next, we shall prove that for MI or MD collision frequencies and equal input pulse areas, the echo amplitude has a single extremum. That is, the echo power has a single bump as τ is increased.

Since the quantity to be measured is $a_1(t = 2\tau,\tau)$ as a function of τ, the derivative of the echo amplitude with respect to τ is given by

$$\frac{da_1(t=2\tau,\tau)}{d\tau} \equiv 2\left.\frac{\partial a_1(t,\tau)}{\partial t}\right|_{t=2\tau} + \left.\frac{\partial a_1(t,\tau)}{\partial \tau}\right|_{t=2\tau} . \qquad \text{(B-7)}$$

Thus,

$$\frac{da_1}{d\tau} = -\frac{1}{\pi}\int_0^{\pi} g(\theta)\, \nu_c(\theta)\, e^{-\nu_c(\theta)\tau}\, d\theta , \qquad \text{(B-8)}$$

from Eq. B-2 with $t = 2\tau$. Next let $\tau = T + \Delta$, where T and Δ are both greater than zero. Then,

$$\frac{da_1}{d\tau} = -\frac{1}{\pi}\int_0^{\theta_c} g(\theta)\, \nu_c(\theta)\, e^{-\nu_c(\theta)T}\, e^{-\nu_c(\theta)\Delta}\, d\theta$$

$$+ \int_{\theta'_c}^{\pi} g(\theta)\, \nu_c(\theta)\, e^{-\nu_c(\theta)T}\, e^{-\nu_c(\theta)\Delta}\, d\theta \qquad \text{(B-9)}$$

For $\nu_c(v)$ MI, and $\Delta > 0$, $e^{-\nu_c(\theta)\Delta}$ is a MI function of θ. Therefore,

$$\int_0^{\theta_c} g(\theta)\nu_c(\theta)e^{-\nu_c(\theta)T}\ e^{-\nu_c(\theta)}\ d\theta$$

$$\leq e^{-\nu_c(\theta_c)\Delta} \int_0^{\theta_c} g(\theta)\ \nu_c(\theta)\ e^{-\nu_c(\theta)\ T} d\theta \quad , \qquad \text{(B-10)}$$

and

$$\int_{\theta_c}^{\pi} g(\theta)\nu_c(\theta)e^{-\nu_c(\theta)T}\ e^{-\nu_c(\theta)\ \Delta} d\theta$$

$$\leq e^{-\nu_c(\theta_c)\Delta} \int_{\theta_c}^{\pi} g(\theta)\nu_c(\theta)\ e^{-\nu_c(\theta)T} d\theta \quad . \qquad \text{(B-11)}$$

Combining results (B-8) to (B-11),

$$\left.\frac{da_1}{d\tau}\right|_{\tau=T+\Delta} \geq e^{-\nu_c(\theta_c)\ \Delta} \left.\frac{da_1}{d\tau}\right|_{\tau=T} \qquad \text{(B-12)}$$

In order to interpret Eq. (B-12) we need a few more results. First, since a_1 is zero for $\tau=0$, and approaches zero as $\tau \to \infty$, by the Mean Value Theorem there must be at least one value of τ between zero and infinity for which $da_1/d\tau$ vanishes. We call the first such time τ_c. Next, for $\nu_c(v)$ MI, $(da_1/d\tau) < 0$ for small τ, as was shown in the last section. Thus, $da_1/d\tau < 0$ for $0 < \tau < \tau_c$. Inserting $T = \tau_c$ into Eq. (B-12) shows that $da_1/d\tau > 0$ for $\tau > \tau_c$. Therefore there can be no more extrema in $a_1(2\tau,\tau)$ as a function of τ. A similar result can be proved for $\nu_c(v)$ MD.

In terms of a two-pulse echo experiment this result implies that the echo power as a function of τ has a single maximum at $\tau = \tau_c$ if $\nu_c(v)$ is a monotonic function, and if the two input pulses have equal area. For $\tau > \tau_c$, the echo power is a MD function of τ.

In this section we wish to relieve the restriction of equal pulse areas. If the two pulses have areas corresponding to electron velocities v_1 and v_2 respectively, Eq. (B-2) is rewritten as

$$a_1(t = 2\tau,\tau) = \frac{1}{\pi}\int_0^{\pi} h(\theta)\, e^{-\nu_c(\theta)\tau}\, d\theta \qquad \text{(B-13)}$$

where $h(\theta) = v_1 \cos 2\theta + v_2 \cos \theta$ is the analog of $g(\theta)$. All of the previous results of this appendix still hold if $h(\theta)$ has only one zero in the interval $(0,\pi)$. This condition is satisfied for $v_2 \geq v_1$, but not for $v_2 < v_1$. The condition $v_2 < v_1$ has its most profound effect on the results formulated in Section III. Namely, for $v_2 < v_1$, even if $\nu_c(v)$ is monotonic, there may be multiple maxima in the echo power as a function of τ. This comes from the possibility of a_1 changing sign.

5. In this section we relieve the restriction of monotonic $\nu_c(v)$, but assume equal pulse areas. Suppose

$$\nu_c(v) = \begin{cases} 0 & v < v_1 \text{ and } v > v_2 \\ 1 & v_1 < v < v_2 \end{cases} \qquad \text{(B-14)}$$

Then

$$\nu_c(\theta) = \begin{cases} 1 & \theta_2 < \theta < \theta_2 \\ 0 & \theta < \theta_2 \text{ and } \theta > \theta_1 , \end{cases} \qquad \text{(B-15)}$$

where $\theta_i = 2 \cos^{-1} (v_1/2v_0)$ from Eq. (8). We assume $v_2 < 2v_0$, where v_0 corresponds to the pulse area, for otherwise $\sigma(v)$ is MI over the velocity range of interest. Putting equation (B-15) into Eq. (B-2) and integrating,

$$a_1(2\tau,\tau) = [1-e^{-\tau}] \Big\{ \sin\theta_1 (\cos\theta_1 + 1) - \sin\theta_2 (\cos\theta_2 + 1) \Big\} \qquad \text{(B-16)}$$

Equation (B-16) shows the usual linear τ dependence for small τ. There may be a zero in a_1 if the term in braces vanishes, but this term is dependent only on the input pulse power (i.e. v_0) and not on τ. Therefore the echo envelope for this type of collision frequency has a characteristic shape, multiplied by a scale factor which is some complicated function of the input pulse power. This unphysical feature is a result of the zero collision frequency over part of the distribution.

6. In this last section we introduce a model which bears a closer relation to the actual collision cross section shown in Fig. 2. The collision frequency to be used is shown as the solid curve in Fig. B2. In terms of the angle, θ, ν_c is expressed as

$$\nu_c = \begin{array}{ll} a & \left\{ \begin{array}{l} \theta_1 < \theta < \theta_2 \\ \theta > \theta_2 \\ \theta < \theta_1 \end{array} \right. \\ b & \\ c & \end{array} \tag{B-17}$$

With this cross section, Eq. (B-2) becomes

$$a_1(2\tau,\tau) = \frac{1}{\pi}\Big[G(\theta_1)(e^{-c\tau} - e^{-a\tau}) + G(\theta_2)(e^{-a\tau} - e^{-b\tau})\Big] \quad , \tag{B-18}$$

where $G(\theta) = \frac{1}{2}\sin 2\theta + \sin\theta$. We have assumed, of course, that $2v_0 > v_1$, for otherwise ν_c is MI over the relevant velocity range $(0 < v < 2v_0)$. If we let b and c go to zero, we obtain the result of Eq. (B-16). If a=c or a=b, ν_c is monotonic, and the results are already known. Another case that is easily handled is a $\gg$ b,c. Then

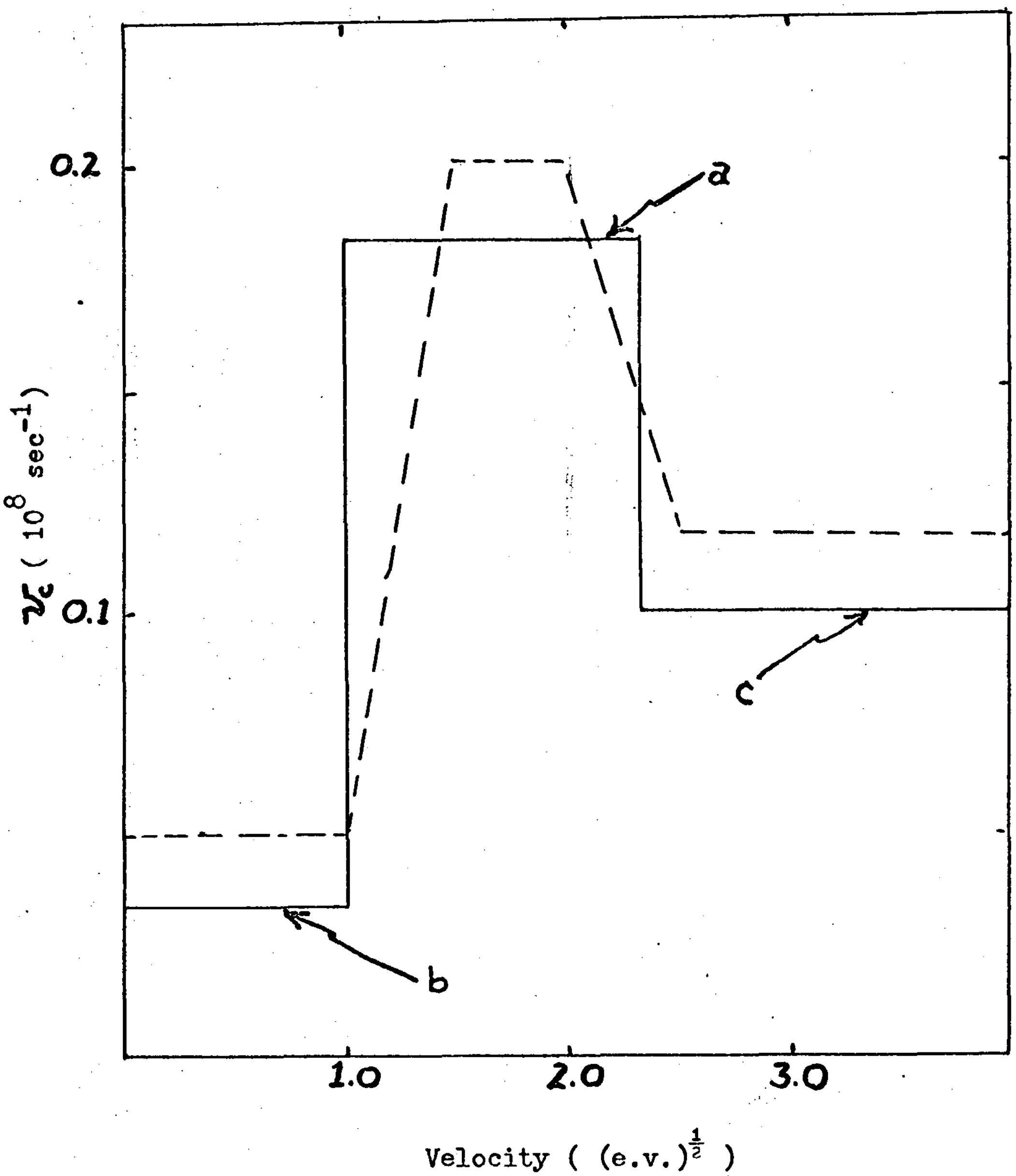

Figure B2. Analytic approximation to the Cs collision frequency.

$$a_1(2\tau,\tau) \approx \frac{1}{\pi}\left(G(\theta_1)e^{-c\tau} - G(\theta_2)e^{-b\tau}\right) \quad . \tag{B-19}$$

A zero in a_1 occurs at τ_c, where

$$\tau_c = \frac{1}{c-b} \ln\left(\frac{G(\theta_1)}{G(\theta_2)}\right) \quad . \tag{B-20}$$

This form shows the qualitative trends in which we are interested. If $2v_0$ is only slightly greater than v_1, and θ_1 is small. Since G is a smooth function with a single peak at $\theta = \pi/3$, unless v_2 is also small (i.e. θ_2 approaches π), the logarithm term of Eq. (B-20) is negative and there is no positive τ_c unless $b > c$. For θ_1 near $\pi/3$ (i.e. $v_0 = v_1/\sqrt{3}$), the logarithm term is positive and a positive τ_c requires $c > b$.

Assuming $c > b$, as the pulse area is increased from $v_0 = 1/2\ v_1$, the log term of Eq. (B-20) starts out negative, passes through zero, increases to a maximum, and then approaches zero again for infinite pulse area. The zero in the echo amplitude for this case starts at $\tau=0$ for a certain threshold pulse area $(G(\theta_1) = G(\theta_2))$. As the pulse area is increased, this zero moves out to greater τ, and turns around and leads back toward $\tau=0$ for large pulse powers. Further, with pulse area held constant, increasing c and b by the same scale factor (i.e. increasing the atom density) decreases τ_c. Decreasing c alone increase τ_c.

Conversely, assuming $c < b$, as the pulse area increases to that corresponding to $v_0 = v_1/2$, a zero appears in the echo envelope at $\tau=\infty$. As the pulse area is increased, τ_c decreases monatonically toward zero. In this case also increasing b and c by the same scale factor decreases τ_c, while decreasing c alone decreases τ_c.

In order to give some support to these qualitative statements, numerical calculations were performed by $a_1(2\tau,\tau)$ by integration on a computer. The collision frequency actually used was that shown dotted in Fig. B2. The numbers were taken to approximate the actual Cs collision frequency for a Cs pressure of 10^{-4} Torr, and a time scale of ten nanoseconds. That is, $\tau=1$ implies $\tau=10$ nanoseconds. The velocities are in units of $(\text{e.v.})^{1/2}$.

Figure B3 shows a typical envelope of the echo power for $v_0 = 1.6$ (greater than half v_1). The zero of the echo amplitude, a_1, shows up as a striking feature in the power ($a_1^{\,2}$) envelope at $\tau=\tau_c$. Figure B4 shows how τ_c increases as the input pulse area is increased above a threshold (in this case, $v_0 \approx 1.19$ $(\text{e.v.})^{1/2}$). Finally, Fig. B5 shows the sensitive dependence of τ_2 on c, the collision frequency on the high velocity shoulder. This figure shows roughly the $1/(c-b)$ dependence predicted in Eq. (B-20).

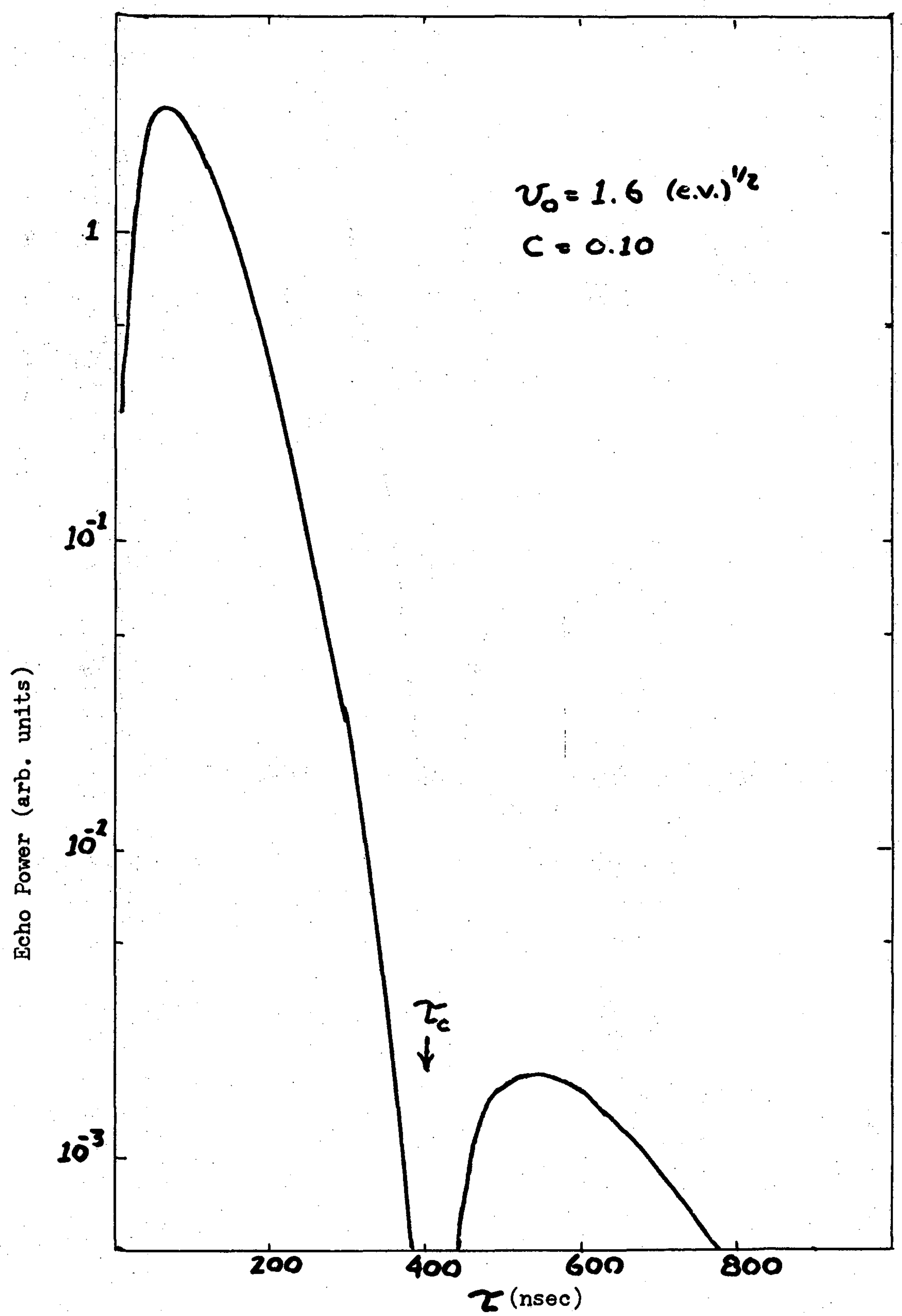

Figure B3. First two-pulse echo power, showing τ_c.

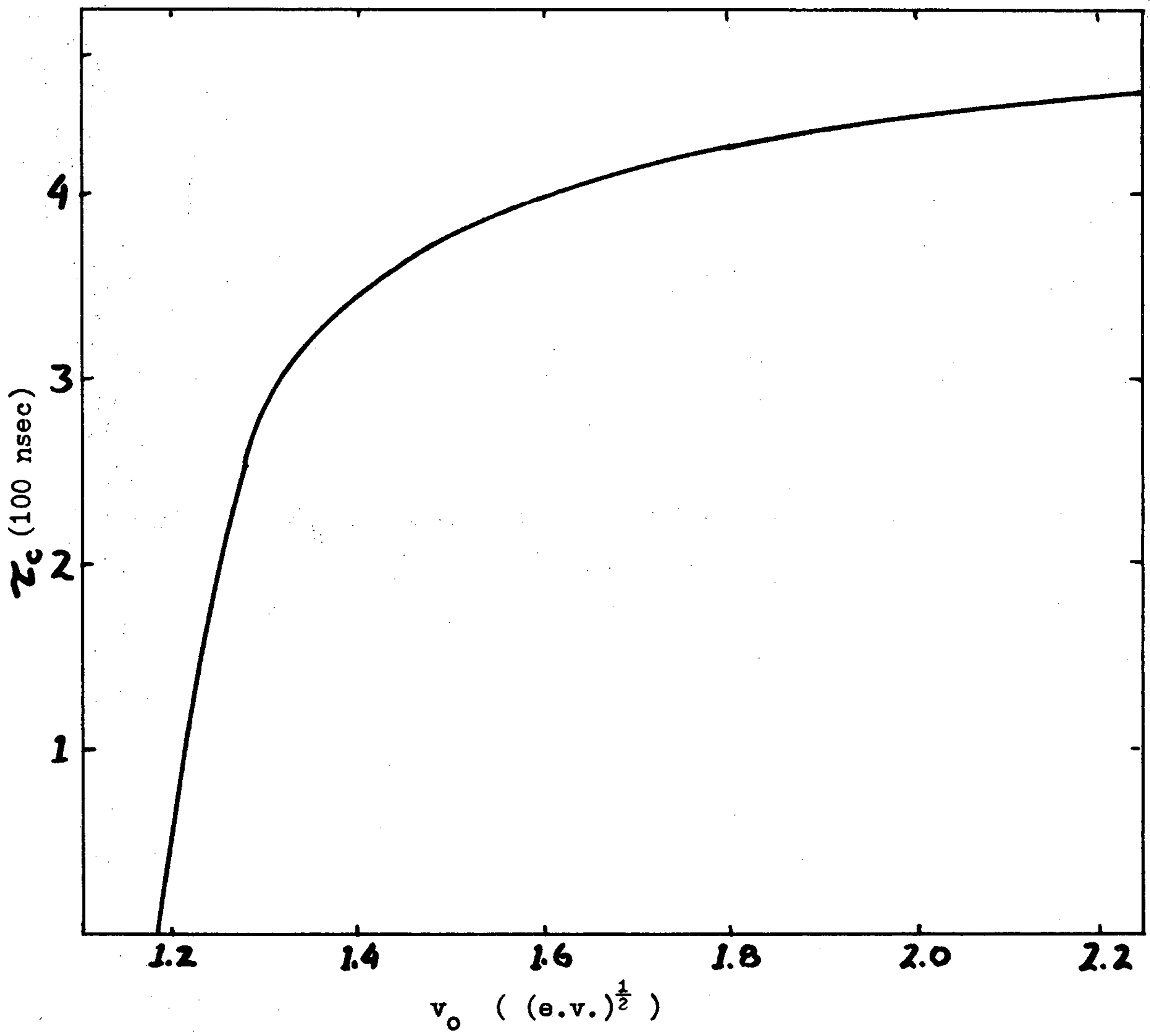

Figure B4. τ_c as a function of v_o using the collision frequency of figure B2 with c = 0.10.

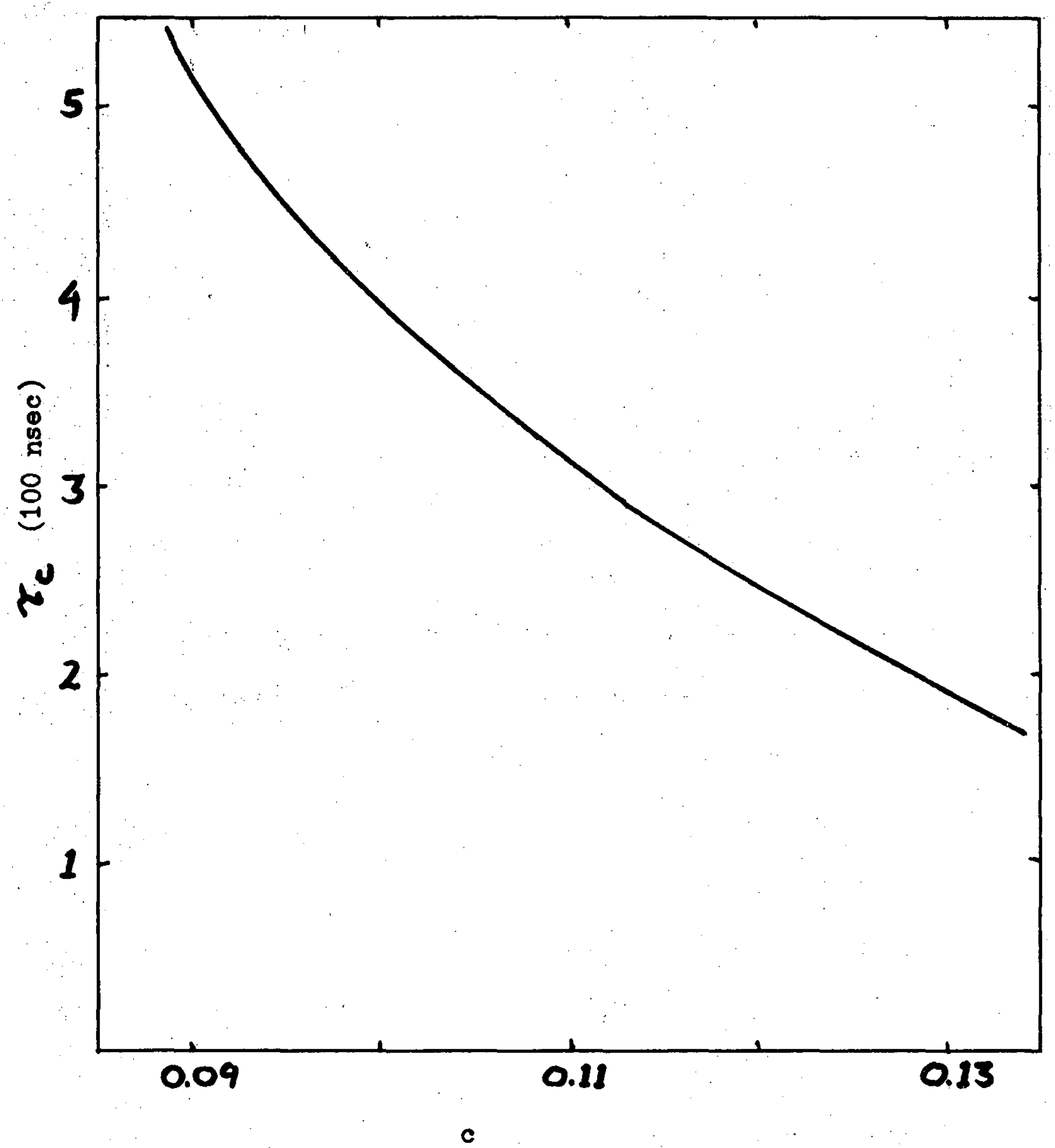

Figure B5. τ_c as a function of c using the collision frequency of figure B2 with $v_o = 1.6$ (e.v.)$^{\frac{1}{2}}$.

APPENDIX C

Multiple Echoes From a Two Level System

In this appendix, we prove that it is in principle possible to get multiple echoes even from a quantum two-level system. To that end, we take a spin 1/2 system, in an inhomogeneous magnetic field. The Hamiltonian for this system is

$$\mathcal{H} = \mathcal{H}_0 + \mathcal{H}_1 \tag{C-1}$$

where $\mathcal{H}_0 = \hbar\omega J_z$, and $\mathcal{H}_1 = \gamma\sigma_x H_x \cos \omega_0 t$, where σ_x is the standard Pauli spin matrix. The ω in $\mathcal{H}_0$ refers to a particular oscillator (or isochromat) in the assumed inhomogeneously broadened line. We make the following rotating frame transformation:

$$\mathcal{H}' = e^{i\omega_0 J_z t} \; \mathcal{H} \; e^{-i\omega_0 J_z t} \tag{C-2}$$

where ω_0 is the frequency of the applied radiation $H_x(t) \cos \omega_0 t$. Then,

$$\mathcal{H}' = \mathcal{H}_0 + 1/2 \; \gamma H_x \; \sigma_x \tag{C-3}$$

where σ_x is the Pauli spin matrix, and we have averaged over ω_0, since the populations change little in one cycle of the radiation. This is the usual procedure of ignoring the non-secular terms, or throwing out the counter-rotating component of H.

The density matrix for a particular isochromat is defined, as usual, by

$$\rho = |\psi\rangle \langle\psi| . \tag{C-4}$$

Then in the rotating frame,

$$\rho' = e^{i\omega_0 J_z t} \; \rho \; e^{-i\omega_0 J_z t} , \text{ or}$$

$$\rho'_{ij} = \overline{c_j^* c_i} \; e^{i\Omega_{ji} t} , \tag{C-5}$$

where c_j is the static part of the amplitude for the jth basis state of the wave function and $\Omega_{ij} = 1/\hbar\ (E_i - E_j) - \omega_0$. The bar indicates an ensemble average over a particular isochromat.

In this reference frame, the equation of motion for the density matrix is

$$i\hbar\dot{\rho}' = [\mathcal{H}'_p, \rho] \tag{C-6}$$

where $\mathcal{H}'_p = \hbar(\omega-\omega_0)J_z + 1/2\ \gamma H_x\ \sigma_x$. When $H_x = 0$, the solutions are simply

$$\begin{aligned} \rho_{11}'(t) &= \rho_{11}'(0) \\ \rho_{22}'(t) &= \rho_{22}'(0) \\ \rho_{12}'(t) &= \rho_{12}'(0)e^{-i\Omega t} \end{aligned} \tag{C-7}$$

where $\Omega = \omega - \omega_0$. In accordance with our usual assumption that the pulse width of incident radiation is smaller than the reciprocal bandwidth of the resonant transition, during a pulse, we shall ignore the term in $\mathcal{H}'_p$ proportional to J_z. Then during a resonant pulse, the density matrix elements which solve (C-6) are:

$$\begin{aligned} \rho_{11}'(t) &= \rho_{11}'(0)\cos^2(\tfrac{1}{2}\theta) + \rho_{22}'(0)\sin^2(\tfrac{1}{2}\theta) \\ &\quad + (\rho_{12}'(0) - \rho_{21}'(0))i\sin(\tfrac{1}{2}\theta)\cos(\tfrac{1}{2}\theta) \\ \rho_{22}'(t) &= \rho_{22}'(0)\cos^2(\tfrac{1}{2}\theta) + \rho_{11}'(0)\sin^2(\tfrac{1}{2}\theta) \\ &\quad + (\rho_{21}'(0) - \rho_{12}'(0)i\sin(\tfrac{1}{2}\theta)\cos(\tfrac{1}{2}\theta) \\ \rho_{12}'(t) &= \rho_{12}'(0)\cos^2(\tfrac{1}{2}\theta) + \rho_{21}'(0)\sin^2(\tfrac{1}{2}\theta) \\ &\quad + (\rho_{11}'(0) - \rho_{22}'(0)i\sin(\tfrac{1}{2}\theta)\cos(\tfrac{1}{2}\theta) \\ \rho_{21}'(t) &= (\rho_{12}'(t)^*) \end{aligned} \tag{C-8}$$

where $\theta = \gamma H_x t$.

The radiation from a particular isochromat with frequency Ω is proportional to $S_x(\Omega)$ for that isochromat, where

$$S_x(\Omega) = \mathrm{Tr}\,(\rho'(\Omega) S'_x).$$

The total radiating moment for the system will be proportional to

$$\langle S_x \rangle = \int_{-\infty}^{\infty} g(\Omega)\ \overline{S_x(\Omega)}\ d\Omega. \tag{C-9}$$

At time t=0 we assume a system in thermal equilibrim, so $\rho_{11} = a$, $\rho_{22} = b$ and $\rho_{12} = 0$. A pulse of angle θ_1 is then applied. For later times

$$\overline{S_x(\Omega)} = -\,1/2\ (b-a)\ \sin\theta_1\ \sin((\omega_0 + \Omega)t),$$

and (C-10)

$$\langle S_x \rangle = -\,1/2\ (b-a)\ \sin\theta_1\ \sin\omega_0 t\ G(t)$$

where G(t) is our usual Fourier transform of the distribution function, and a symmetric line has been assumed.

If a second pulse, with area corresponding to an angle θ_2, is applied at $t = \tau$, then for $t > \tau$,

$$\begin{aligned}\overline{S_x(\Omega)} = {} & -\,1/2\ (b-a)\ \sin\theta_1\ \cos^2(1/2\ \theta_2)\ \sin((\omega_0+\Omega)t) \\ & +\ 1/2\ (b-a)\ \sin\theta_1\ \sin^2(1/2\theta_2) \times \sin(\omega_0 t + \Omega(t-2\tau)) \\ & -\ 1/2\ (b-a)\ \cos\theta_1\ \sin\theta_2\ \sin(\omega_0 t + (t-\tau))\end{aligned} \tag{C-11}$$

Then,

$$\begin{aligned}\langle S_x \rangle = {} & -1/2\ (b-a)\ \sin\omega_0 t\ \{\ \sin\theta_1\ \cos^2(1/2\theta_2)\ G(t) \\ & +\ \cos\theta_1\ \sin\ {}_2\ G(t-\tau) \\ & -\ \sin\theta_1\ \sin^2(1/2\theta_2)\ G(t-2\tau)\ \}.\end{aligned} \tag{C-12}$$

The first term in the braces corresponds to the usual free induction tail from the first pulse; the second term corresponds to a free induction tail from the second pulse; the third term corresponds to the echo at $t = 2\tau$. This is the same as Hahn's original classical result,[3] but without relaxation.

Before including relaxation, we shall restrict the pulse so that $\theta_1 = \theta_2 = \pi/2$. Then the last term of Eq. (C-11) is zero (no free induction decay after the second pulse), and the other two terms can be combined to give the total transverse component of the spin (S_x for $\sin((\omega_0+\Omega)t) = 1$) for the Ω isochromat as

$$|S_t| \propto (\cos 2\,\Omega\tau - 1). \qquad \text{(C-13)}$$

Since the transverse component of the spin is the radiating part, we see that two 90° pulses introduce a periodic modulation on the strength of the radiation from the spin system. The lack of higher order echoes at $t = n\tau$, $n = 3, 4 \ldots$, then, is just a manifestation of the lack of higher order Fourier components in Eq. (C-13).

To bring this system closer to cyclotron echoes, we introduce a phenomenological T_2 process which will depend on the magnitude of the transverse spin component. This process is accounted for by multiplying the off diagonal terms of the density matrix by e^{-t/T_2}. Since $|S_t|$ is constant over the spectrum after the first 90° pulse, for $0 < t < \tau$ the relaxation term is an overall damping factor, and will be ignored. For $t > \tau$, $|S_t|$ has the periodicity indicated by Eq. (C-13), and so will $e^{-(t-\tau)/T_2}$. If we now write

$$e^{-(t-\tau)/T_2} = \Sigma\, a_n\, e^{+in\Omega\tau}, \qquad \text{(C-14)}$$

and multiply the off diagonal density matrix elements by this sum, then Eq. (C-12) becomes

$$\langle S_x \rangle = -1/4\ (b-a)\ \sin \omega_0 t\ \ \Sigma\, a_n[G(t-n\tau) + G(t - (n+2)\tau)]. \tag{C-15}$$

Thus, multiple echoes are possible. In this calculation the implict assumption was made that T_2 remains constant, even though $|S_t\ (\Omega)|$ is changing. In realisitic cases this will not be true, and the problem would have to be solved self-consistantly.

APPENDIX D

A Criterion for Spin and Cyclotron Echoes

We rewrite Eq. (19) for the case where Ω for a given electron is time dependent. Let the frequency $\Omega = \Omega\,(x,t)$, where x is a spacial coordinate locating the oscillator.

$$\tilde{P}\,(t > \tau) \;=\; v_0 e^{\nu_0 \tau}$$

$$\times \int \left(\exp\left[i \int_0^{\tau} \Omega\,(x,t')\,dt'\right] + \left(\exp\left[-\int_{\tau}^{t} \nu_c(x)\,dt'\right]\right)\right. \tag{D-1}$$

$$\times \exp\left[i \int_{\tau}^{t} \Omega\,(x,t')\,dt'\right] g\,(x)\,dx$$

Let $\int_0^{\tau} \Omega(x,t')\,dt' = \bar{\Omega}\,(x)\tau$. Then the first and second terms inside the integral (C-1) are periodic in $\bar{\Omega}$, since ν_c depends only on the electron velocity after the second pulse, and therefore on $\bar{\Omega}$.

Therefore, we may make the substitution of Eq. (20) to get

$$P \;=\; v_0 e^{-\nu_0 \tau}\; \Sigma\, a_n \int e^{-in\,\bar{\Omega}\,(x)\tau}$$
$$\times \;\exp\left[i \int_{\tau}^{t} \Omega(x,t')\,dt'\right] g(x)\,dx. \tag{D-2}$$

Assuming τ is much greater than the electron spectral line width, the integral in Eq. (D-2) is seen to average to zero unless

$$\int_{\tau}^{t} \Omega(x,t')\,dt' \;=\; n\,\bar{\Omega}\,(x)\tau \tag{D-3}$$

for nearly all x. If Eq. (D-3) is satisfied for some t and for all x, then an echo, with an amplitude dependent on a_n, can be expected at that t. Obviously, if Ω (x) is constant in time, then this condition predicts echoes at $t = n\tau$ as in Eq. (22). Condition D-3 also holds for spin echoes. For example, if one doubles the inhomogeneity in the magnetic field at $t = \tau$, one expects the echo rephasing to occur earlier than $t = 2\tau$. Equation (D-3) in this case reads

$$2 \ \Omega (x) (t-\tau) = h \ \Omega (x)\tau, \text{ or } t = \frac{3}{2} \ \tau$$

for the time of the echo. (In this case the only non-zero fourier amplitudes, a_n, are $n = 0, 1$.)

REFERENCES

1. Ovid, Metamorphoses, translated by R. Humphries (Indiana U. Press, 1958) p. 68.
2. T. Bulfinch, The Age of Fable (Sanborn, Carter and Bozin, Boston, 1855) p. 141.
3. E. L. Hahn, Phys. Rev., 80,580 (1950).
4. R. J. Blume, Phys. Rev. 109, 1867 (1958). J. P. Gordon, K. D. Bowers Phys. Rev. Lett. 1, 368 (1958).
5. I. Solomon, Phys. Rev. 110, 61 (1958).
6. N. A. Kurnit, I. D. Abella, and S. Hartmann, Phys. Rev. Lett. 13, 567 (1964). I. D. Abella, et al.,Phys. Rev. 141, 391 (1966). C. K. N. Patel, and R. E. Slusher, Phys. Rev. Lett. 20, 1087 (1968).
7. B. Bolger, J. C. Diels, Phys. Lett. 28A, 401 (1968).
8. R. M. Hill, et al, Phys Rev. Lett. 18, 105 (1967).
9. J. L. Kenkins and P. E. Wagner, Applied Phys. Lett., 13, 308 (1968).
10. S. A. Miller, Thesis, Univ. of Calif. Berkeley (unpublished). J. W. Shaner, S. A. Miller and E. L. Hahn, Bull. Am. Phys. Soc, Series II, 13, 358 (1968).
11. R. P. Feynman, J. App. Phys. 28, 49 (1957).
12. C. P. Slichter, Principles of Magnetic Resonance (Harper and Row, N. Y. , 1963) p. 16.
13. R. M. Hill, D. E. Kaplan, Phys. Rev. Lett. 14, 1062 (1965). G. F. Herrman, R. M. Hill and D. G. Kaplan, Phys. Rev 156, 118 (1967).
14. F. E. Kaplan, Phys. Rev. Lett 14, 254 (1965)
15. J. H. Malmberg, et al., Phys Rev. Lett. 20, 95 (1968). J. H. Malmberg, et al., Phys. Fluids 11, 1147 (1968).

16. H. Ikezi and N. Takahashi, Phys. Rev. Lett. 20, 140 (1968). D. R. Baker, et al, Phys. Rev. Lett 20, 318 (1968).

17. R. W. Gould, Phys. Lett 19, 477 (1965).

18. W. H. Kegel and R. W. Gould, Phys. Lett 19, 531 (1965).

19. F. W. Crawford and R. S. Harp, J. App. Phys. 37, 4405 (1966).

20. R.S. Harp, R. L. Bruce, and F. W. Crawford, J. App. Phys. 38, 3385 (1967).

21. D. E. Kaplan , R. M. Hill and A. Y. Wong, Phys. Lett. 22 585 (1966).

22. A. Abragam, Principles of Nuclear Magnetism (Oxford Univ. Press, London, 1961) p.33.

23. R. B. Brode, Rev. Mod. Phys. 5, 257 (1933).

24. C. L. Chen and M. Raether, Phys. Rev 126, 2679 (1962).

25. C. Ramsauer, Ann d. Physik 69, 513 (1921), Ann d. Physik 66, 545 (1921), Ann d. Physik 72, 345 (1923).

26. W. P. Allis and P. M. Morse, Z. Physik 70, 567 (1931).

27. C. E. Moore, Atomic Energy Levels, Vol. III (NBS Circular No. 467 1958) p. 125.

28. K. Rubin, et al. Phys. Rev 117, 151 (1951).

29. S. C. Brown, Basic Data of Plasma Physics (Technology Press, MIT Cambridge, 1959) p. 31.

30. E. Karule and R. Peterkop in IVth International Conference on the Physics of Electronic and Atomic Collisions (Science Book Crafters, N. Y., 1965).

31 M. A. Heald and C. B. Wharton, Plasma Diagnostics with Microwaves, (John Wiley and Sons, N. Y. , 1965) p. 81.

32. R. W. Gould, Phys. Lett. 29A, 347 (1969).

33. G. N. Watson, A Treatise on the Theory of Bessel Functions, (Cambridge Univ. Press, Cambridge, England, 1944) p. 15.

34. R. L. Aggarwal, M. Zuteck, and B. Lax, Phys. Rev. Lett 19, 236 (1967).

35. S. L. McCall and E. L. Hahn, Phys. Rev. Lett 18,908 (1967).

36. J. P. Gordon and K. S. Bowers, Phys. Rev. Lett 1, 368 (1958).

37. M. Weger, PhD. Thesis, University of Cal., Berkeley, (unpublished).

38. W. Feller, An Introduction to Probability Theory and Its Applications I (John Wiley and Sons, N. Y. 1950) p. 325.

39. J. L. Delcroix, Introduction to the Theory of Ionized Gases, (Interscience Publ. N. Y., 1960) p. 80

40. Ibid., p. 91.

41. J. Crank, The Mathematics of Diffusion (Oxford Univ. Press, London 1956) p. 13.

42. M. A. Heald and C. B. Wharton, op. cit., p 1.

43. Ibid, p. 35.

44. Ibid, p. 82

45. C. J. Smithells, Metals Reference Handbook, (Butterworth, London, 1955).

46. J. W. Shaner and E. L. Hahn (to be published) (UCRL-19063).

TECHNICAL INFORMATION DIVISION
LAWRENCE RADIATION LABORATORY
UNIVERSITY OF CALIFORNIA
BERKELEY, CALIFORNIA 94720